Important Notice

THE UNIVERSITY OF CALGARY

Pseudo-Spectral Modelling of Cracked Anisotropic Media

and Rotation of Multicomponent Shear-Wave Data

by

Kangan Fang

A THESIS

SUBMITTED TO THE FACULTY OF GRADUATE STUDIES

IN PARTIAL FULFILLMENT OF THE REQUIREMENTS FOR THE

DEGREE OF MASTER OF SCIENCE

DEPARTMENT OF GEOLOGY AND GEOPHYSICS

CALGARY, ALBERTA

NOVEMBER, 1998

THE UNIVERSITY OF CALGARY

FACULTY OF GRADUATE STUDIES

The undersigned certify that they have read, and recommend to the Faculty of Graduate Studies for acceptance, a thesis entitled "Pseudo-spectral modelling of cracked anisotropic media and rotation of multicomponent shear-wave data" submitted by Kangan Fang in partial fulfillment of the requirements for the degree of Master of Science.

Supervisor, Dr. R. J. Brown

Department of Geology and Geophysics

Dr. E. S. Krebes

Department of Geology and Geophysics

Dr. G. F. Margrave

Department of Geology and Geophysics

Dr. M. A. Slawinski

Department of Mechanical Engineering

November 30, 1998

Date

ABSTRACT

Cracked anisotropic media are modelled with Hudson's theory and the pseudo-spectral method is used to do the numerical simulation of wave propagation in anisotropic media. New algorithms for the rotation of both the multisource multireceiver (MSMR) and single-source multireceiver (SSMR) shear-wave data are developed and tested on both the synthetic data and field data.

The new algorithm for the rotation of the MSMR data can deal with the situation where the two sources have different wavelet signatures. The rotation algorithms can be used to scan for the rotation parameters, the rotation angle and the time lag between the fast and slow waves. After rotation, the fast and slow shear waves are separated and the attributes of azimuthal anisotropy are estimated.

ACKNOWLEDGMENTS

TABLE OF CONTENTS

LIST OF FIGURES

Chapter 1: Introduction

1.1 Background

Multicomponent exploration has turned out promising results and gained an increasing interest in the exploration industry and university community. The primary reason for this development is the conviction that since seismic particle motion is vector (three-component) in nature, full recording and processing of it will provide more geological information and better understanding of the Earth (Stewart, 1994). The availability of multicomponent data makes it possible for anisotropy to be investigated. Seismic anisotropy is the phenomenon in which the properties of a medium, such as elastic-wave velocities, vary with the direction of observation. The use of multicomponent seismic exploration technology and the study of anisotropy has allowed geophysicists to obtain more information about the properties of the Earth, such as lithology, porosity, fracture orientation and fracture density. Multicomponent seismic data are generated by either one or two shear-wave sources or by conversion of P waves from a compressional source.

1.1.1 Anisotropy and shear-wave splitting

It is now commonly believed that most upper-crustal rocks are anisotropic to some degree (Crampin, 1981). The presence of anisotropy in the Earth, which manifests itself most diagnostically in terms of shear-wave splitting in multicomponent seismic data, can lead to substantial complication in the processing and interpretation of both surface seismic and VSP shear-wave data. However, analysis of anisotropic wave-propagation phenomena, such as shear-wave splitting, or birefringence, could lead to more information, such as strike direction and density of vertical fractures within reservoirs (Lynn, et al., 1995; Winterstein and Meadows, 1991) to help in the understanding of the Earth.

Anisotropy may be caused by fine layering in sedimentary rocks, by preferred crystal orientation in crystalline solids, by preferred orientation of grains in sedimentary rocks, or by stress-aligned fractures or cracks (e.g. Crampin, 1981 and references therein). Transverse isotropy with vertical symmetry axis (TIV) is the most extensively studied anisotropy type. It serves as a good introduction to anisotropy for geophysicists and helps define the basic terminology and methodology for anisotropy studies (Winterstein, 1990). Azimuthal anisotropy is of special interest to explorationists because it is commonly related to vertical fractures or cracks.

In an azimuthally anisotropic medium, the only shear waves that will propagate are those polarized in the natural polarization directions intrinsic to the medium, i.e. the directions parallel and perpendicular to the strike of fractures (Thomsen, 1988). Therefore, a source vector will be vectorially decomposed into the two principal components. The component polarized parallel to fracture strike (fast wave) will travel faster than the other component, which is polarized perpendicular to it (slow wave). This phenomenon is called shear-wave splitting or birefringence. The fast and slow shear waves will arrive at a receiver at different times, which usually will degrade the data quality and make processing and interpretation more difficult. However, through so-called rotation of multicomponent shear-wave data, it is possible to separate the fast and slow shear waves and to obtain certain attributes of the fractures, such as the strike direction and density of fractures (e.g. Esmersoy, 1990).

1.1.2 Shear-wave rotation

Shear-wave rotation refers to the rotation of the acquisition coordinate system into a natural coordinate system for receivers, sources or both. After rotation, the data look like they would if we had conducted the acquisition along a natural coordinate system, as defined in the previous section. Ideally, the fast and slow waves can be fully separated; the strike direction of vertical fractures can be determined, and the density of the fractures can be estimated from the time lag between the fast and slow waves.

Many rotation algorithms have been proposed and used in the analysis of shear-wave data, such as: Alford's (1986) algorithm; rotation by hodogram analysis method

(e.g. Schulte and Edelmann, 1988); Esmersoy's (1990) algorithm based on inversion and the algorithms based upon either the autocorrelation or crosscorrelation of rotated components (Narville, 1986; Peron, 1990; Harrison 1992). Each of these methods applies to different situations and assumes different conditions. Thomsen's (1988) algorithm, which was derived from a different point of view, is essentially the same as Alford's. In this thesis, new algorithms for the rotation of multisource multireceiver (MSMR) and single-source multireceiver (SSMR) shear-wave data are investigated. These new methods can deal with the situation where the two sources have different wavelet signatures (for the MSMR case) and are robust in the presence of noise.

1.1.3 Modelling the azimuthal anisotropy

In principle, any elastic medium can be fully characterized by its stiffness tensor, which relates the nine components of the strain tensor to the nine components of the stress tensor in Hooke's law. Due to symmetry properties, only 21 of 81 stiffness coefficients are independent in a homogeneous elastic medium (Winterstein, 1990). For a medium that belongs to a special symmetry class, the number of independent stiffness coefficients will be reduced accordingly. For example, a TI medium can be represented by 5 independent stiffness coefficients (Thomsen, 1986).

For the azimuthal anisotropy caused by vertical fractures, it is very natural to relate the stiffness tensor to the crack density. Hudson (1981, 1982) has presented a theory to compute the stiffness tensor given a crack density, which allows us to model the azimuthal anisotropy by adding first and second order perturbations to the stiffness tensor of the uncracked medium.

1.1.4 Numerical modelling of wave propagation in azimuthally anisotropic media

Numerical modelling is very useful in the study of anisotropy. It can help in the interpretation of field data. It is also often used to generate synthetic test data in theoretical studies. Almost every method used for isotropic modelling can be used for anisotropic modelling. These methods include ray tracing (Guest and Thomson, 1993), the finite-difference method (Carcione, 1990; Dong and McMechan, 1995; Faria and

Stoffa, 1994) and the pseudo-spectral method (Kosloff and Carcione, 1989; Lou and Rial, 1995). Due to the complexity of anisotropy, a major concern in numerical modelling of anisotropy is the heavy computation load. Therefore, the pseudo-spectral method is chosen here to do the numerical modelling of azimuthal anisotropy, because of its fast computation speed.

1.2 Some fundamental concepts

1.2.1 Crack density, ξ

This thesis is mainly concerned with the azimuthal anisotropy caused by a uniform distribution of parallel vertical fractures or cracks as shown in Figure 1.1. By parallel vertical fractures, it is meant that their strike directions are parallel and that the normals to the fracture surfaces are horizontal. In Chapter 2, this kind of azimuthal anisotropy is modelled by computing the effective stiffness tensor from the Lamé constants, λ and μ, of the uncracked medium and the crack density, ξ, using Hudson's (1981, 1982) theory. Here, the concept of crack density is adapted from Crampin (1984), which is defined as $\xi = Na^3/v$, where N is the number of circular cracks of radius a in volume v. In Hudson's (1981, 1982) original definition, he called N/v the number density of cracks, which is natural and understandable. Crampin's (1984) crack density definition can be justified in the sense that it is dimensionless and can be regarded roughly as a qualitative measure of the ratio of total crack volume to the total volume of the medium. Whatever it is called, ξ is a proper measure of the intensity of cracks. Because Hudson's (1981, 1982) expressions for stiffness perturbations contain the same parameter combinations as the parameter ξ, it is also natural to choose such a definition of crack density.
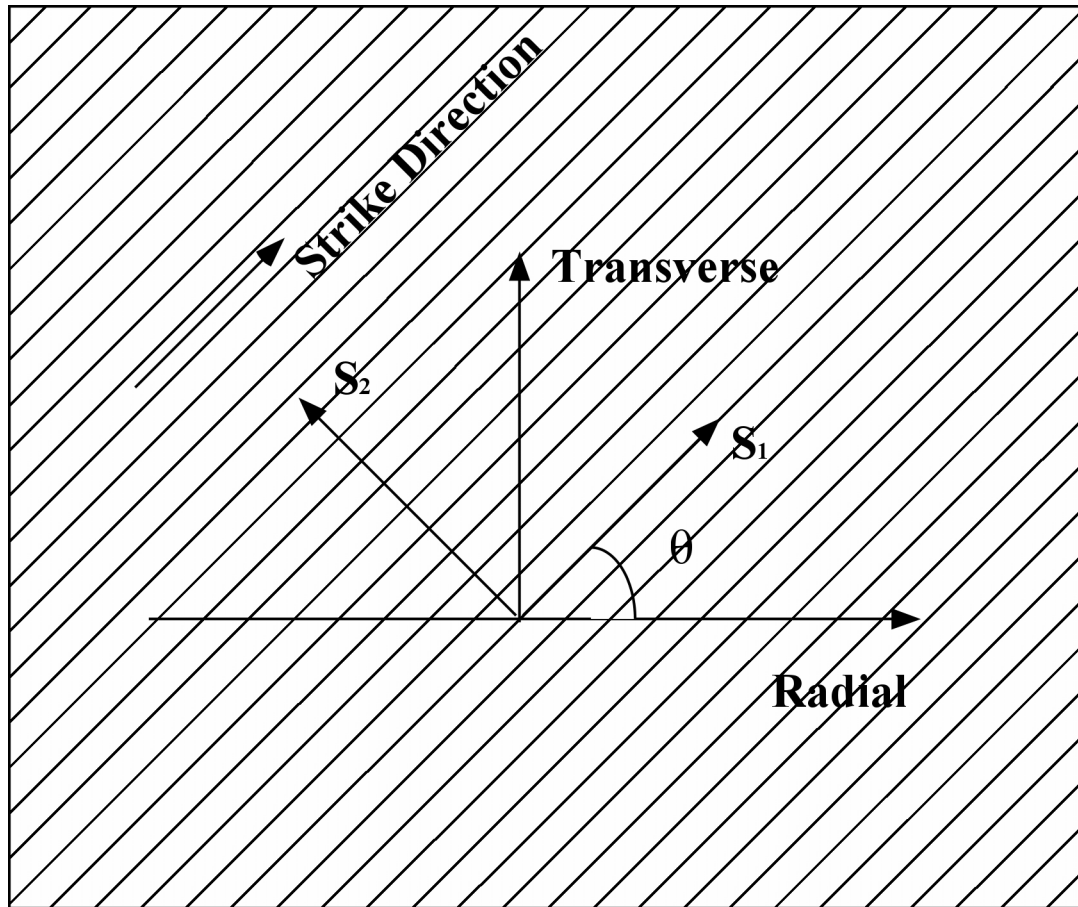
Figure 1-1. Illustration of fractured media; S_1 is the direction of polarization of the fast shear waves and S_2 the polarization direction of the slow waves.

1.2.2 Phase velocity and group velocity

In anisotropic media, wavefronts travelling outward from a point source are not, in general, spherical as a result of dependence of velocity upon direction of propagation. Shown in Figure 1-2 are two wavefronts in space that are separated by unit time. The group velocity, $V(\phi)$, denotes the velocity with which energy travels from the source, while the phase velocity, $v(\varphi)$, is the velocity with which a wavefront propagates at a local point, that is, the propagation velocity of the parallel plane-wave component. Here, ϕ is the group angle, also called ray angle, and specifies the direction of the ray from the

source point to the point of interest. And φ is the phase angle, also called wavefront-normal angle; it specifies the direction of the vector that is normal to the wavefront. Since the wavefront is not spherical, it is apparent that phase angle is, in general, different from group angle at any point of propagation, except at certain singular points.
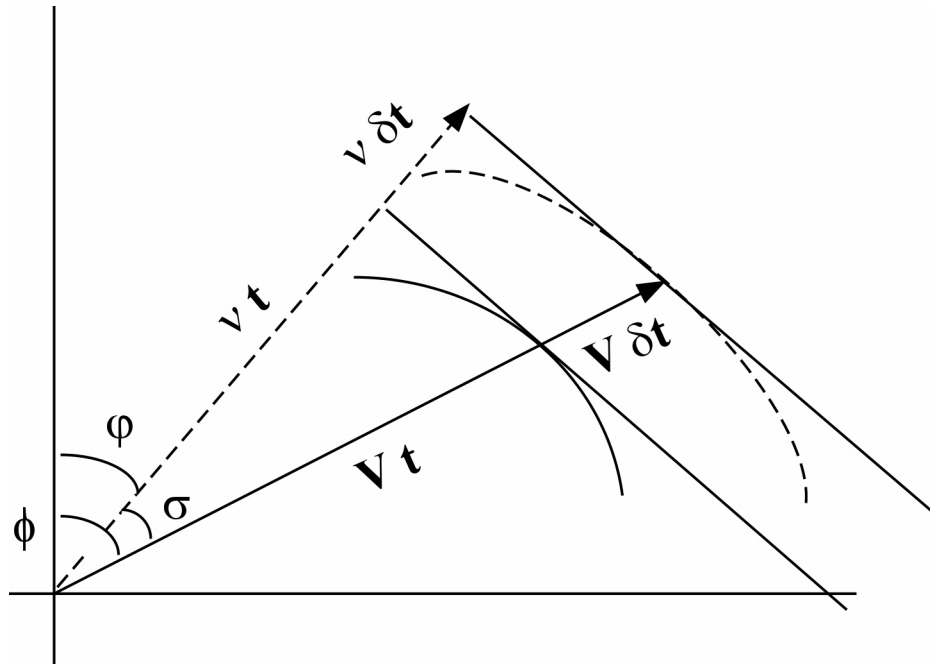
Figure 1-2. Illustration of phase angle, φ, group angle, ϕ, phase velocity, $v(\varphi)$, and group velocity, $V(\phi)$.

Now, as shown in Figure 1-2, define $\sigma = \phi - \varphi$. It can be shown that (Berryman, 1979):

$$\cos\sigma = \frac{v}{V} \qquad (1\text{-}1)$$

and that:

$$\tan\sigma = \frac{1}{v}\frac{dv}{d\varphi} \qquad (1\text{-}2)$$

Following from the trigonometric identities:

$$\tan[\phi(\varphi)] = \tan(\varphi+\sigma) = \frac{\tan\varphi + \tan\sigma}{1 - \tan\varphi\tan\sigma} \qquad (1\text{-}3)$$

and

$$\left(\frac{V}{v}\right)^2 = \sec^2\sigma = 1 + \tan^2\sigma, \qquad (1\text{-}4)$$

the relationship between group angle and phase angle can be expressed as:

$$\tan[\phi(\varphi)] = \left(\tan\varphi + \frac{1}{v}\frac{dv}{d\varphi}\right) \bigg/ \left(1 - \frac{\tan\varphi}{v}\frac{dv}{d\varphi}\right), \qquad (1\text{-}5)$$

and the scalar magnitude V of the group velocity is given in terms of the phase-velocity magnitude v by:

$$V^2[\phi(\varphi)] = v^2(\varphi) + \left(\frac{dv}{d\varphi}\right)^2. \qquad (1\text{-}6)$$

1.2.3 Rotation angle, θ, and time lag, Δ

As mentioned in section 1.1.1 and 1.1.2, a shear wave will split, in general, into two orthogonally polarized shear waves, a fast wave and a slow wave, in the presence of azimuthal anisotropy (Figure 1.1). The polarization directions of the two shear waves resulting from splitting are called natural polarization or coordinate directions (Winterstein, 1990) if they are used to define a natural coordinate system, as opposed to the acquisition coordinate system. In multisource shear-wave acquisition, the acquisition coordinate system is defined by the polarization directions of the radial (inline) and

transverse (crossline) shear-wave sources. In cracked media, the fast wave is generally polarized along the strike direction of the parallel vertical fractures. Rotation angle refers to the angle between the polarization direction of the fast wave and the radial (inline) direction of the acquisition system. Time lag is the difference of the traveltimes of the fast and slow shear waves arriving at a particular point. The determination of these two parameters is the key issue in the rotation of shear-wave data.

1.3 Objectives of the thesis

This thesis work is concerned with the rotation of the horizontal components of shear-wave data, both for the MSMR case and for the SSMR case (e.g. P-SV data). The goal is to develop new rotation algorithms that are robust and suitable for both the MSMR case, where the two shear-wave source signatures are not necessarily identical, and the SSMR case. The algorithms will be tested on both synthetic data and field data.

Hudson's theory is used to model the azimuthal anisotropy caused by vertical fractures. The effective stiffness tensor computed is in turn used in the numerical modelling of anisotropy to generate synthetic data for the testing of the rotation algorithms.

1.4 Data sets used in the thesis

The algorithms for the rotation of the MSMR and SSMR shear-wave data are tested and evaluated with the data sets described below.

1.4.1 Synthetic data sets generated by the ray-tracing method

The data sets used in Figure 4-2 through Figure 4-7 and in Figures 5-1 and 5-2 were created by simple ray-tracing (geometrical seismology) according to the mechanism of the vertical shear-wave splitting.

The wavelets used are Ricker wavelets with dominant frequencies of 30 to 50 Hz.

1.4.2 Synthetic data sets generated by pseudo-spectral numerical modelling

The data sets used in Figure 4-8 through Figure 4-10 and in Figures 5-3 and 5-4 are created by the pseudo-spectral numerical modelling described in Chapter 3.

1.4.3 The Olds 9C-2D data set

The field data used in Chapter 4 is a 9C-2D data set acquired by the Amerada Hess Corporation Limited in the area of Olds, Alberta in 1993. Greater details is given by Yang (1996).

1.5 Hardware and software used

The thesis research work was conducted on a Sun Microsystems network operated by The CREWES Project of The Department of Geology and Geophysics at the University of Calgary. Thesis typing and image processing were done using Microsoft Word and Canvas on a PC computer.

The pseudo-spectral numerical modelling program was coded using ANSI Fortran language. All other programs were coded using Matlab 4.0. All the image graphics were created using Matlab and screen captured by the Grabwindow program. The ProMAX seismic data processing system and the XV program were also used to view the images.

Chapter 2:   Modelling cracked media

2.1 Introduction

A common case of azimuthal anisotropy encountered in hydrocarbon exploration is the anisotropy caused by stress-aligned vertical fractures or cracks (Crampin and Lovell, 1991). The determination of strike direction and density of the fractures is of great interest to explorationists. Because the elastic properties of an elastic medium are fully defined by its stiffness tensor, to model azimuthal anisotropy caused by vertical cracks, we need to relate the stiffness tensor to crack density. Hudson (1981, 1982) investigated the stiffness tensor computation in cracked elastic media. With his theory, the effective stiffness tensor can be computed by adding a first-order and a second-order perturbation to that of the uncracked medium. The perturbations can be computed from the crack density and the stiffness tensor of the uncracked medium. Crampin (1984) computed the stiffness tensor in two-phase media to model the attenuation of seismic waves in anisotropic media. With the stiffness tensor defined, it is possible for us to simulate the wave propagation through an anisotropic medium by numerical modelling.

Thomsen (1986) introduced three anisotropic parameters, ε, δ and γ, to describe weak anisotropy, which is believed to be a common case in anisotropy. These parameters can be computed from the stiffness tensor of the anisotropic medium. In turn, phase and group velocities can be computed with the Thomsen anisotropic parameters.

2.2 The effective stiffness tensor in cracked media

Suppose that we have an isotropic medium with Lamé constants, λ and μ. We introduce into it a weak distribution of parallel penny-shaped cracks to make it anisotropic. The cracks are specified by the crack orientation and the so-called crack density, $\zeta = Na^3/v$ ($\zeta << 1$), where N is the number of cracks of radius a in volume v. Hudson (1981, 1982) presented an expression for the effective stiffness tensor in cracked media for long-wave length seismic waves as (Crampin, 1984):

$$C_{ijkl} = C_{ijkl}^0 + C_{ijkl}^1 + C_{ijkl}^2 \qquad (2\text{-}1)$$

where C_{ijkl}^0 is the stiffness tensor of the uncracked medium, C_{ijkl}^1 and C_{ijkl}^2 are the first- and second-order perturbations of the isotropic elastic constants. The first- and second-order perturbations are computed with the crack density and the Lamé constants.

Using this equation, we can determine an expression for an anisotropic medium by, in effect, introducing a set of cracks through the effective stiffness tensor.

The stiffness tensor in four-index notation can be converted to and from two-index notation by the Voigt recipe (Cheadle et al., 1991):

$$C_{ijkl} \Leftrightarrow C_{\alpha\beta}$$

where $\alpha = i$ for $i = j$; and $\alpha = 9 - (i + j)$ for $i \neq j$; and for β, just replace i, j with k, l.

Expressed in two-index notation, the stiffness tensor of an isotropic medium is:

$$C_{\alpha\beta}^0 = \begin{pmatrix} \lambda+2\mu & \lambda & \lambda & & & \\ & \lambda+2\mu & \lambda & & & \\ & & \lambda+2\mu & & & \\ & & & \mu & & \\ & & & & \mu & \\ & & & & & \mu \end{pmatrix} \tag{2-2}$$

where components equal to zero are omitted. The stiffness tensor of a transversely isotropic medium with vertical symmetry axis is:

$$C_{\alpha\beta} = \begin{pmatrix} C_{11} & (C_{11}-2C_{66}) & C_{13} & & & \\ & C_{11} & C_{13} & & & \\ & & C_{13} & & & \\ & & & C_{44} & & \\ & & & & C_{44} & \\ & & & & & C_{66} \end{pmatrix} \tag{2-3}$$

and the first-order perturbation is:

$$C_{\alpha\beta}^1 = \begin{pmatrix} \lambda^2 & \lambda^2 & \lambda(\lambda+2\mu) & & \\ & \lambda^2 & \lambda(\lambda+2\mu) & & \\ & & (\lambda+2\mu)^2 & & \\ & & & \mu^2 & \\ & & & & \mu^2 \end{pmatrix} \bullet D \bullet \left(-\frac{\xi}{\mu}\right) \tag{2-4}$$

where D = diag $(U_{11}, U_{11}, U_{11}, U_{33}, U_{33}, 0)$, and U_{11} and U_{33} can be computed from the Lamé constants of the uncracked medium (Crampin, 1984). For dry cracks:

$$U_{11} = \left(\frac{4}{3}\right)\frac{\lambda + 2\mu}{\lambda + \mu}, U_{33} = \left(\frac{16}{3}\right)\frac{\lambda + 2\mu}{3\lambda + 4\mu}. \tag{2-5}$$

Therefore, we are able to compute the effective stiffness tensor from the Lamé constants of the uncracked medium and the crack density.

Because the so-called crack density is small ($\ll 1$), the second-order perturbation, which is proportional to its square, is neglected.

2.3 Rotation of the coordinate system

Using Hudson's theory, the stiffness tensor of a cracked TIV medium can be computed. Then, the stiffness tensor of a transversely isotropic medium with horizontal symmetry axis (TIH), which is azimuthally anisotropic, can be obtained by rotating the coordinate system.

Rotation of the coordinate system is performed on the stiffness tensor in four-index notation, C_{ijkl}.

The components of the stiffness tensor in four-index notation with respect to the new coordinate system, x_i, in terms of the components in the old coordinate system, x'_p are (Helbig, 1994):

$$C_{ijkl} = \left(\partial x_i / \partial x'_p\right)\left(\partial x_j / \partial x'_q\right)\left(\partial x_{ki} / \partial x'_r\right)\left(\partial x_l / \partial x'_s\right)C'_{pqrs}. \tag{2-6}$$

2.4 The Thomsen anisotropic parameters

With the stiffness tensor obtained from Hudson's theory, we can compute the Thomsen anisotropic parameters and phase and group velocities. For the case of weak anisotropy, the anisotropic parameters are (Thomsen, 1986):

$$\varepsilon = \frac{C_{11} - C_{33}}{2C_{33}}, \quad \gamma = \frac{C_{66} - C_{44}}{2C_{44}}, \quad \delta = \frac{(C_{13} + C_{44})^2 - (C_{33} - C_{44})^2}{2C_{33}(C_{33} - C_{44})}. \qquad (2\text{-}7)$$

2.5 Phase velocity and group velocity

Phase velocities of P, SV and SH waves for weak anisotropy can be computed from the Thomsen parameters (Thomsen, 1986) using the approximate equations:

$$v_P(\varphi) = \alpha_0 \left(1 + \delta \sin^2 \varphi \cos^2 \varphi + \varepsilon \sin^4 \varphi\right) \qquad (2\text{-}8\text{-}1)$$

$$v_{SV}(\varphi) = \left[1 + \frac{\alpha_0^2}{\beta_0^2}(\varepsilon - \delta)\sin^2 \varphi \cos^2 \varphi\right] \qquad (2\text{-}8\text{-}2)$$

$$v_{SH}(\varphi) = \beta_0 \left(1 + \gamma \sin^2 \varphi\right) \qquad (2\text{-}8\text{-}3)$$

where α_0 and β_0 are velocities of P and SH waves along the vertical directions (Figure 2-1). In turn, group velocities can be computed from phase velocities using the theory presented in section 1.2.2.
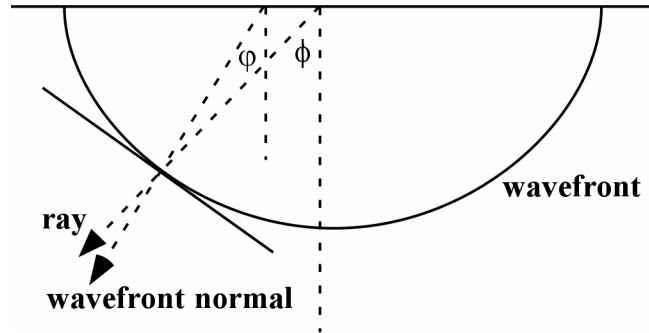
Figure 2-1. Illustration of ray, wavefront, phase angle, φ, and group angle, ϕ, in TIV media.

2.6 Modelling example

Now, we model a TIV medium, i.e., one that is transversely isotropic with a vertical symmetry axis, by introducing a uniform distribution of parallel cracks into an isotropic medium. The P-wave velocity of the uncracked medium is 5800 m/s and V_P/V_S =1.75 before the introduction of cracks, which are assumed to be dry.

Figure 2-2 shows the Thomsen anisotropic parameters versus crack density. All three parameters are nearly linear in crack density when it is small (from 0 to about 0.02).
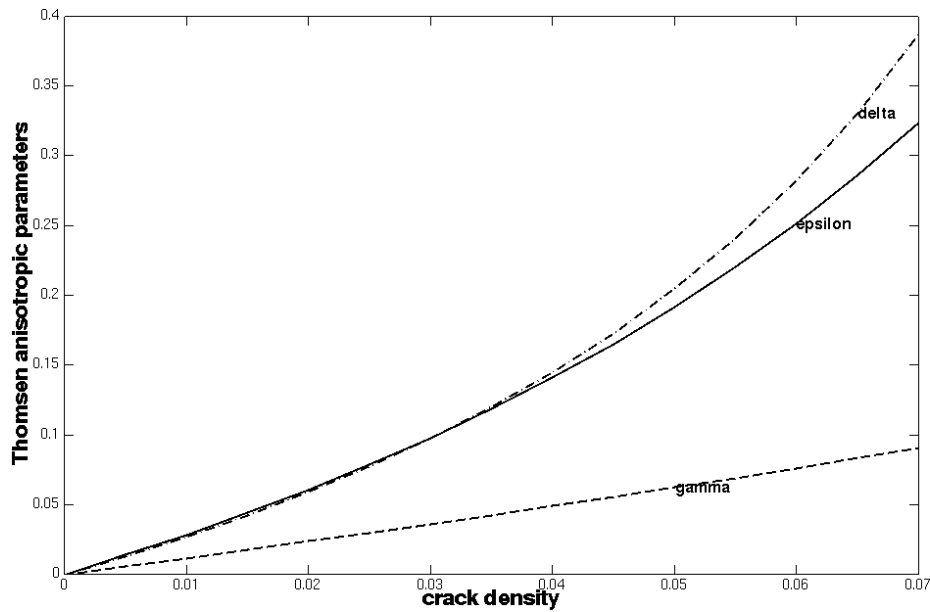
Figure 2-2. Thomsen anisotropic parameters versus crack density in a TIV medium.

Phase velocities of P, SV and SH waves, v_P, v_{SV} and v_{SH}, versus crack density and phase angle, computed from Hudson's (1981, 1982) theory are shown in Figure 2-3 (a), (b) and (c). Also shown is the ratio of SV-wave group velocity to phase velocity, V_{SV}/v_{SV}, versus phase angle (Figure 2-3(d)). Phase velocities decrease with increasing crack density. Note that phase velocity of SV waves reaches a minimum at a phase angle of 45°. Here, both the polarization direction and the ray direction are at 45° to the fast direction, the horizontal direction, and both play a role in reducing SV-wave velocity. The ratio of group velocity to phase velocity is very close to 1 in this range of crack density. All the velocities are computed using the approximate expressions (2-8) for weak anisotropy given by Thomsen (1986). If crack density is increased, absurd values of velocities will be resulted, which indicates that the values of the crack density are out of the range of weak anisotropy.
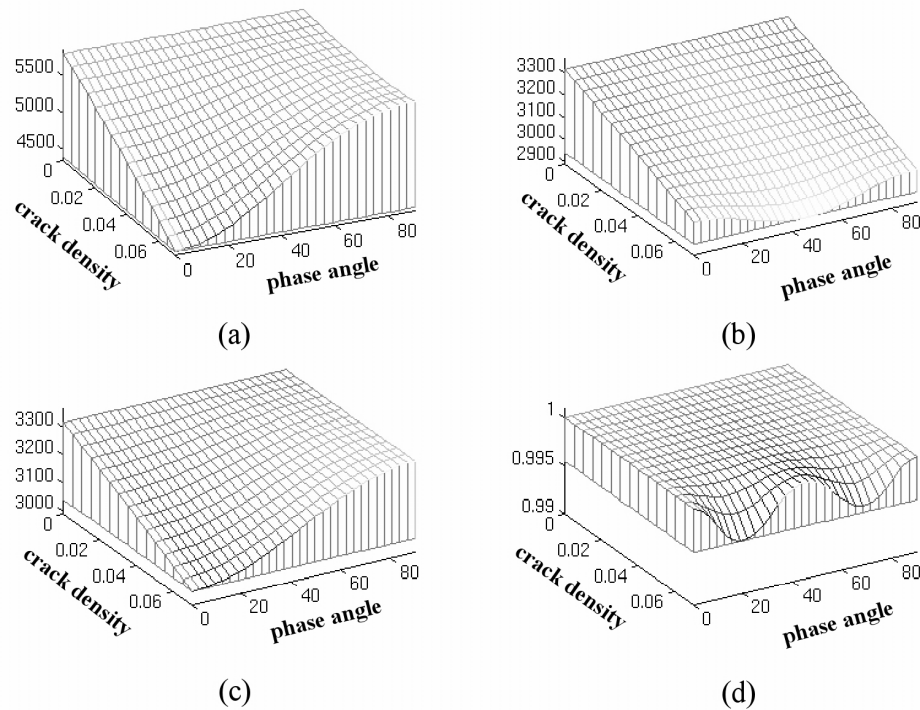
Figure 2-3. (a-c) Phase velocities of P, SV and SH waves, v_P, v_{SV} and v_{SH}, respectively, versus crack density and phase angle; (d) the ratio of group to phase velocity of SV wave, V_{SV}/v_{SV}, versus crack density and angle.

Figure 2-4 (a), (b) and (c) show variations of phase velocities of P, SV and SH waves versus phase angle, computed from the Hudson theory. Each curve represents a different crack density. Figure 2-4 (d) shows the ratio of SV-wave group to phase velocity versus crack density, where each curve represents a different value of phase angle. In Figure 2-4 (d), we can see that group and phase velocities are very nearly equal in the weak-anisotropy range.
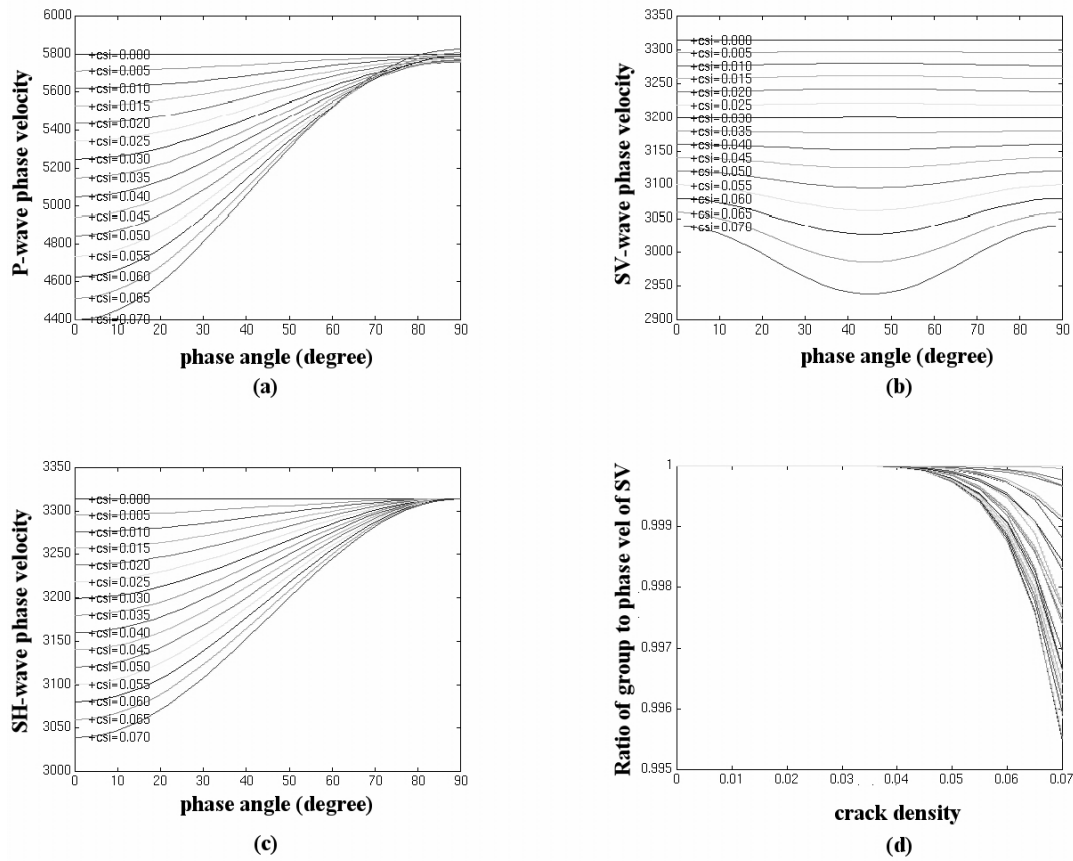
Figure 2-4. (a-c) Phase velocities of P, SV and SH waves, v_P, v_{SV} and v_{SH}, versus phase angle. (d) Ratio of group to phase velocity of SV-wave, V_{SV}/v_{SV}, versus crack density. Computed from the theory of Hudson (1981, 1982).

2.7 Summary

Using Hudson's theory, we can compute the stiffness tensor in cracked media, and hence the Thomsen anisotropic parameters, as a function of crack density and direction of propagation. This provides us with the possibility of relating the phase and group velocity directly to crack density in the cracked medium. Theoretical computation shows that the

weak-anisotropy assumption is valid at small crack density and linearity can be a good approximation for the Thomsen anisotropic parameters. By further applying Hudson's (1981, 1982) theory, we could also examine the velocity variations due to the inclusion of fluids in the cracks. In addition, the velocities computed here can be used to verify the rotation parameters picked by scanning, a topic that is introduced and discussed in Chapter 4.

Chapter 3: Numerical modelling of azimuthal anisotropy

3.1 Introduction

Numerical simulation or forward modelling of wave propagation is an efficient method to produce test data and examine the mechanism of wave propagation. It is also very useful in the interpretation of real data. Due to the complexity of anisotropy, analytical solutions are usually not available. Physical and numerical modelling are necessary means for the analysis of wave propagation in anisotropic media. However, the numerical method is usually preferred when physical modelling is relatively expensive and restrictive.

Many algorithms have been proposed and used for the modelling of anisotropy in the last decades, including ray-tracing methods (Guest and Thomson, 1993), finite-difference methods (Carcione, 1990; Dong and McMechan, 1995; Faria and Stoffa, 1994) and the pseudo-spectral method (Kosloff and Carcione, 1989; Lou and Rial, 1995). Because of the huge computation needed in the numerical modelling of anisotropy, the pseudo-spectral method is preferred over other methods because it is much faster (Lou and Rial, 1995).

The pseudo-spectral method uses the Fourier transform to compute the spatial derivatives and the finite-difference method to compute the time derivative. Compared to other methods, the pseudo-spectral method is fast, accurate and easy to implement. It has been successfully used in the numerical modelling of isotropic media (Gazdag, 1981; Kosloff et al., 1984). Lou and Rial (1995) successfully used the pseudo-spectral method to compute wavefields in 2-D inhomogeneous anisotropic media.

3.2 Principles of pseudo-spectral forward modelling

The equation governing wave propagation in elastic media is:

$$\rho \ddot{u}_i = C_{ijkl} u_{k,lj} + \rho g_i \tag{3-1}$$

where ρ is mass density, u_i is the infinitesimal displacement vector, $u_{k,lj}$ is the partial derivative of u_k with respect to x_l and x_j, C_{ijkl} is the stiffness tensor, and g_i are the body forces per unit mass (Cheadle et al., 1991). Also, C_{ijkl} relate the stress tensor, σ_{ij}, and strain tensor, ε_{kl}, by Hooke's law:

$$\sigma_{ij} = C_{ijkl} \varepsilon_{kl} \tag{3-2}$$

To compute spatial derivatives of displacements by Fourier transformation, we forward-transform the displacements from the space domain into the wavenumber domain, perform complex multiplication, then reverse-transform back to the space domain. For example, consider the derivative

$$\frac{\partial^2 u_k}{\partial x_j \partial x_l} = -\left(\frac{1}{2\pi}\right)^3 \int_{-\infty}^{+\infty} (k_j)(k_l) U_k(k_i) \exp(-ik_i x_i) dk_i \tag{3-3}$$

where $U_k(k_i)$ is the Fourier transform of $u_k(x_i)$, which can be calculated by a 3-D FFT, and k_i is the circular wavenumber in the x_i direction.

Based on the second-order finite-differencing approximation of $\ddot{u}_i$ in equation (3-1), the displacement $u_i(t + \Delta t)$ can be expressed as:

$$u_i(t + \Delta t) = (\Delta t)^2 \ddot{u}(t) + 2u_i(t) - u_i(t - \Delta t) \tag{3-4}$$

where Δt is the sampling interval in time.

The energy source in the modelling is simulated by introducing a force at the source point and in its vicinity. The source force gradually decreases to zero away from the source point to prevent aliasing (Lou and Rial, 1995).

By multiplying by a weighting function to cause the wavefields to attenuate when approaching the model boundary, edge-reflection effects can be greatly reduced. The exponential function proves to be a good weighting function (Cerjan et al., 1985).

Though the pseudo-spectral method is relatively fast, it is still not practical to run 3D anisotropic modelling on a Sun workstation because of the excessive computation time needed.

3.3 2D anisotropic numerical modelling examples and analysis

2D modelling assumes that the model is two-dimentional, say in the (x_1, x_3) plane, or that it is infinite and identical along the x_2 direction and that the sources are line sources extended along the x_2 direction. This can be a good approximation to use to model a medium with vertical fractures. Two model examples are presented below. In discussing the modelling result, symbol u_{ij} will be used to designate displacements computed instead of symbol u_i (vector) that has been used in the previous sections of this Chapter. In symbol u_{ij}, j represents the source polarization direction and i the receiver polarization direction.

3.3.1 Model 1: Homogeneous azimuthally anisotropic model

Model 1 is a homogeneous azimuthally anisotropic model created by introducing a set of vertical fractures or cracks whose strike direction is at an angle ζ to the x_1 direction. Vertical fractures or cracks are assumed to be planar penny-shaped and the normal to the plane of the fractures or cracks is horizontal. The crack density is 0.07 and $\zeta = 45°$. Other parameters are shown in Figure 3-1. The model is 256 grid points by 256

grid points in size, with the grid size being 25 m by 25 m. A source polarized in the x_2 direction is introduced at grid point (128, 25). The time step (sampling interval) is 2 ms. The stiffness tensor for a TIV medium is computed by Hudson's theory (Hudson, 1981, 1982; Crampin 1984) as discussed in Chapter 2, and then transformed to that of TIH (azimuthally anisotropic) medium by coordinate system rotation (Helbig 1994).
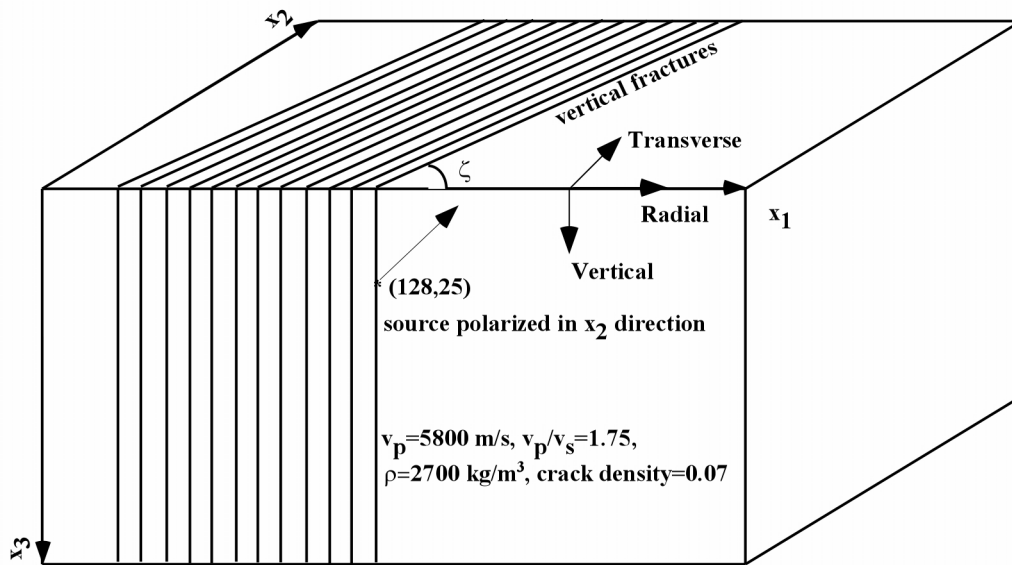
Figure 3-1. Homogeneous azimuthally anisotropic model generated by introducing a set of uniform vertical fractures into an isotropic medium, with the parameters used in the numerical modelling.

Shown in Figure 3-2 are the snapshots of the wave propagation in this model at travel-times of 800, 1200 and 1600 ms for the displacements in both the x_1 and x_2 directions, u_{12} and u_{22}, computed using the pseudo-spectral method discussed in the previous sections. Due to the shear-wave splitting in azimuthally anisotropic media, waves are also recorded in the x_1 direction for a source polarized in the x_2 direction. As propagation time increases, fast and slow waves are separated.
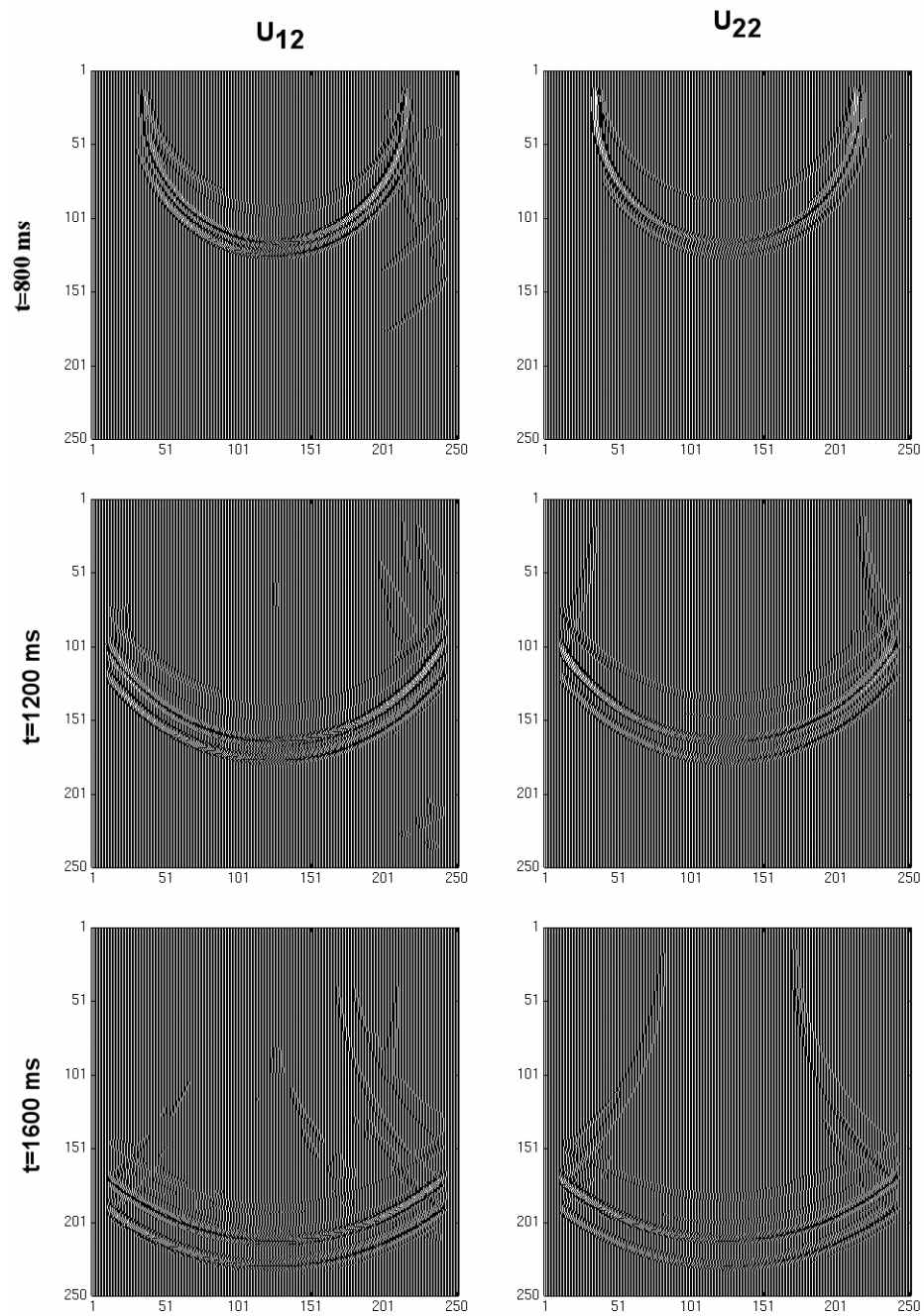
Figure 3-2. Snapshots of wavefield displacements, u_{12} and u_{22}, in the x_1 and x_2 directions, respectively, with source polarized in the x_2 direction. The vertical and horizontal axes give numbers of grid intervals in the x_3 and x_1 directions, respectively.
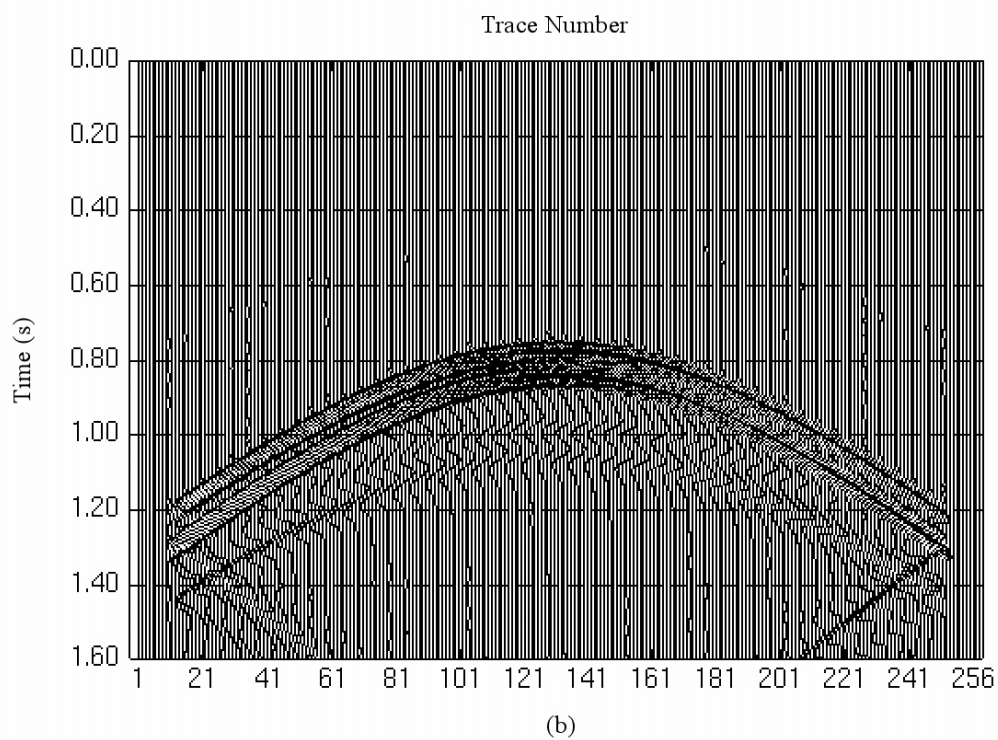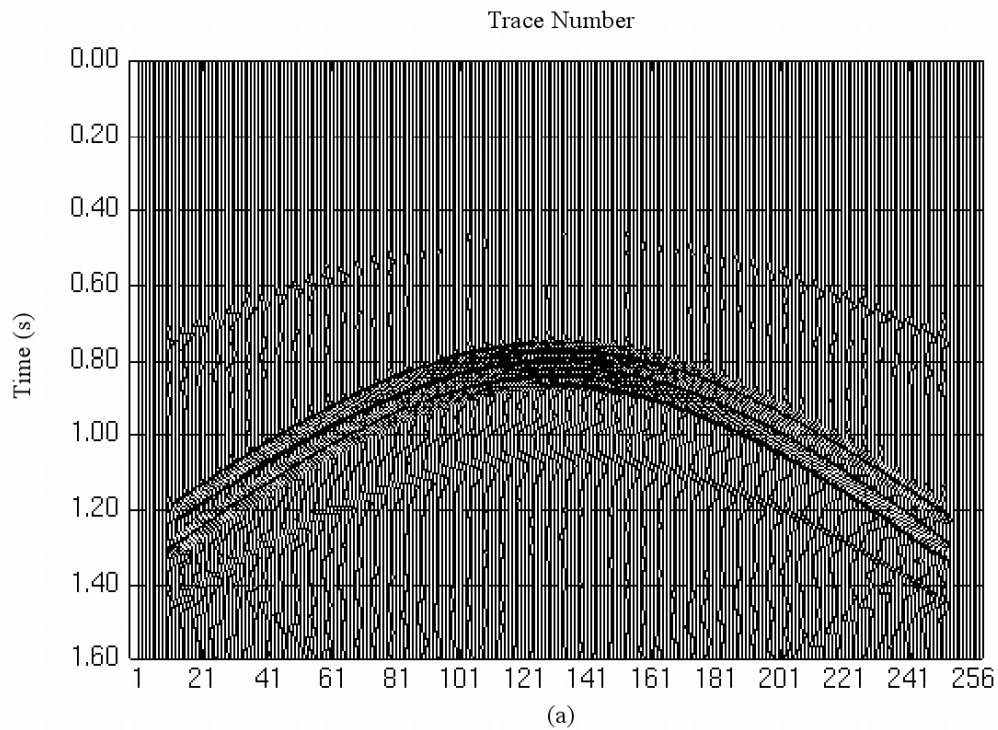
Figure 3-3. Two sections hypothetically recorded along a line at $x_3 = 125$ for both wavefields in the x_1 and x_2 directions; (a) u_{12} and (b) u_{22}.

Figure 3-3 shows two sections hypothetically recorded along a line at $x_3 = 125$ grid intervals for displacement wavefields in both the x_1 and x_2 directions, u_{12} and u_{22}. On both sections, P waves, fast and slow shear waves, and reflections from the free surface are recorded. There are also edge-reflection effects in the sections, due to incomplete elimination of edge effects.
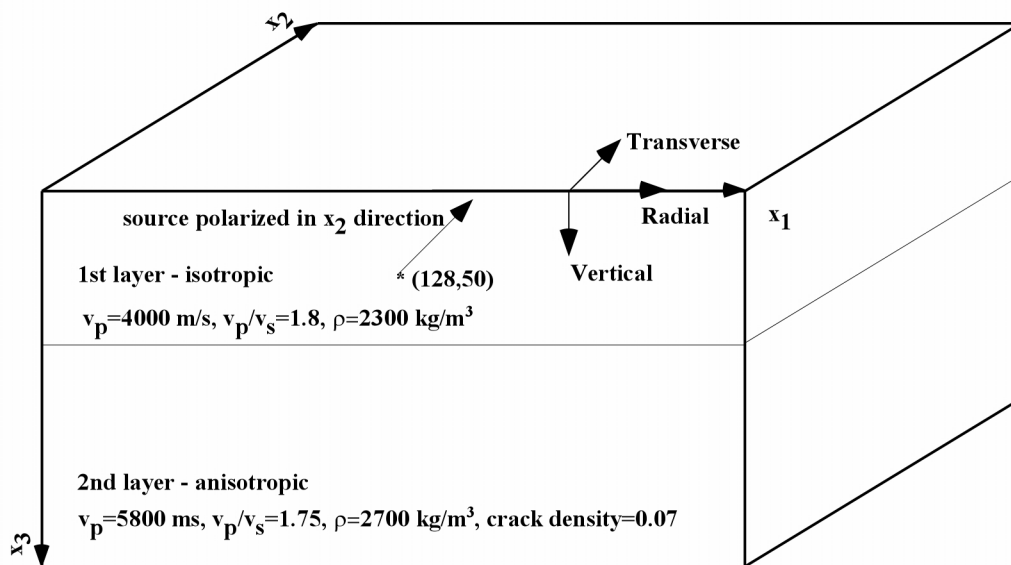
Figure 3-4. Two-layer model, the first layer being isotropic and the second anisotropic, with the parameters used in the numerical modelling.

3.3.2 Model 2: Two-layer azimuthally anisotropic model

Shown in Figure 3-4 is a two-layer model, the first layer being isotropic and the second being anisotropic. The anisotropic layer has the same parameters as Model 1, while the parameters of the isotropic layer are shown (Figure 3-4). The interface between the two layers is located at $x_3 = 100$ grid intervals. The source, which is in the isotropic layer, is polarized in the x_2 direction. Figure 3-5 shows snapshots of wave propagation for displacements u_{12} and u_{22} in the x_1 and x_2 directions respectively. We can see that when no waves have reached the second layer, there is only displacement in the x_2 direction. Upon the propagation of waves into the second layer, the anisotropic layer, shear-wave splitting start to occur and displacements are recorded in the x_1 direction as well as the x_2 direction.

U_{12} U_{22}

t=400 ms

t=800 ms

t=1200 ms
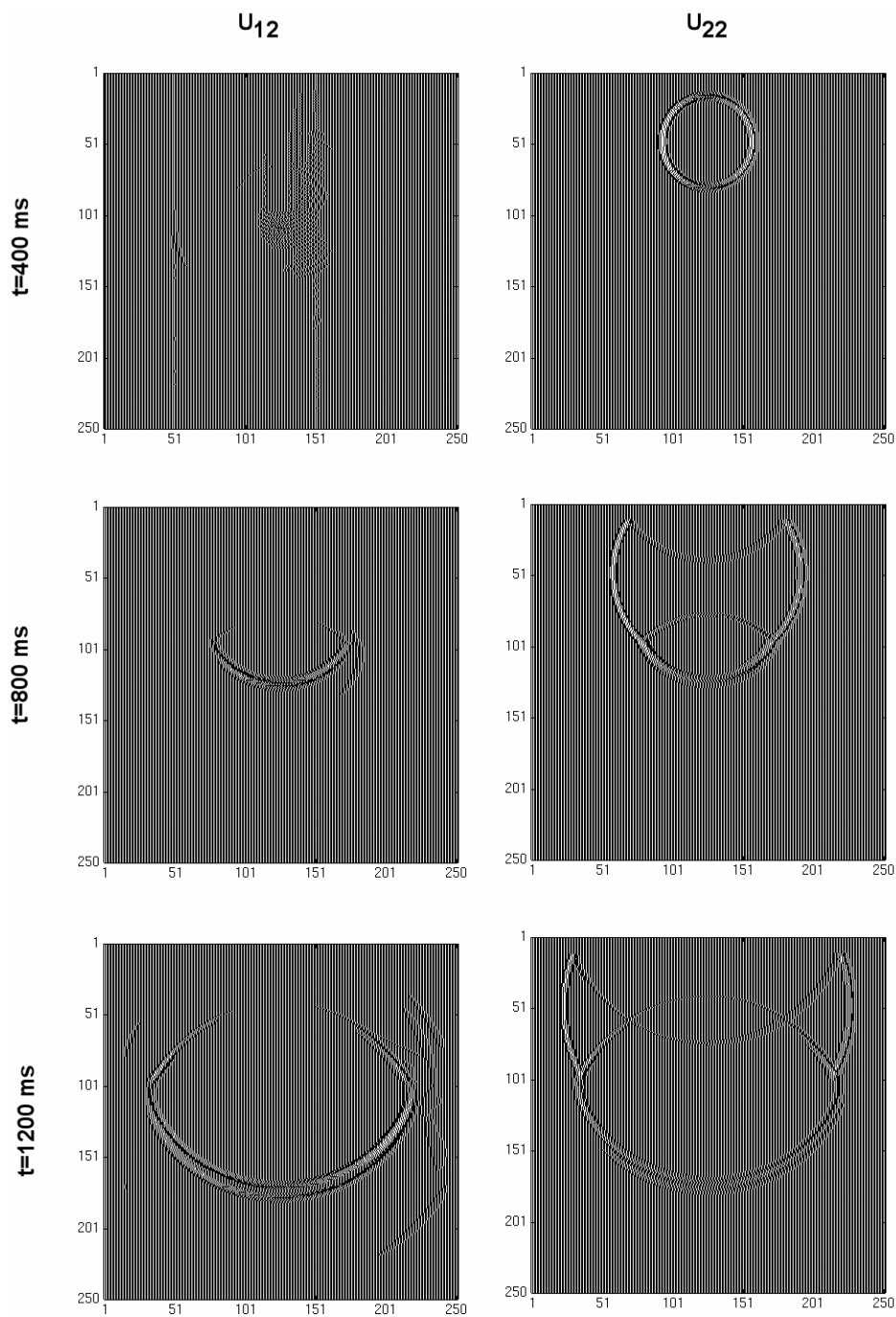
Figure 3-5. Snapshots of wavefield displacements in the x_1 and x_2 directions, respectively, u_{12} and u_{22}, with source polarized in the x_2 direction, for the model shown in Figure 3-4.

3.4 Summary

The pseudo-spectral method proves to be successful in modelling wave propagation in 2D anisotropic media. It is much faster than many other methods (Lou and Rial, 1995 and references therein), accurate, and easy to implement. However, it also has some disadvantages, such as wavenumber dispersions and difficulty in the elimination of edge effects because of its periodic boundary conditions. Though it is feasible to do 3D anisotropic modelling on a supercomputer, it is impractical to realize it on a workstation under present conditions. This simulation algorithm will be used to generate 2D test data for the rotation algorithms discussed in Chapters 4 and 5.

Chapter 4:   Rotation of MSMR shear-wave seismic data

4.1 Introduction

Shear-wave splitting is considered by many to be the most diagnostic phenomenon caused by azimuthal anisotropy (e.g. Crampin, 1981). It may also degrade the quality of shear-wave data and cause mis-ties (Alford, 1986). However, we can obtain the attribute information of anisotropy, such as natural polarization directions and degree of anisotropy, by analyzing shear-wave splitting. Rotation of horizontal components of shear-wave data is one of the key processing procedures in anisotropy analysis. Through rotation, the effect of anisotropy can be compensated for and the fast and slow shear waves can be separated. In the case of azimuthal anisotropy caused by vertically aligned fractures or cracks, the strike of the fractures or cracks and the time lag between the fast and slow waves can be determined by shear-wave rotation, which can be of great interest to exploration geophysicists.

Several algorithms for the rotation of shear-wave seismic data have been devised. Alford's algorithm is intended especially for four-component rotation analysis and it can determine the orientation of the natural coordinate system (Alford, 1986). However, it requires that the two sources have the same wavelet signature. It has been shown that, for data acquired with a single source polarization, such as converted-wave data, Alford's rotation method requires modifications (Thomsen, 1988).

Much work has been done using hodogram analysis methods to study shear-wave splitting (e.g., Schulte and Edelmann, 1988). As discussed by Winterstein (1989), these methods require both very high signal-to-noise ratio and the presence of a single wavelet within the analysis window in order to be effective.

Other two-component birefringence-analysis schemes that do not involve hodograms have largely been based upon either the autocorrelation or crosscorreation of

rotated components (Narville, 1986; Peron, 1990). Harrison (1992) presented an algorithm using the autocorrelation and crosscorrelation of rotated radial and transverse components, which is particularly suitable for converted waves and is robust in the presence of noise. Esmersoy (1990) presented an algorithm to obtain the rotation parameters by an inversion method.

In this chapter, a new algorithm for the rotation of shear-wave data is proposed. This new algorithm can be used to rotate the horizontal components of shear-wave data generated by multiple sources that have different amplitudes and wavelets in azimuthally anisotropic media. Synthetic data tests and a field data example show that the algorithm is successful and robust. The new algorithm is similar to Alford's rotation algorithm, but it involves two parameters, the natural polarization direction angle and the time lag between the fast and slow shear waves, which can be determined by scanning, rather than only one parameter, the former, in Alford's rotation.

4.2 Mathematical background

Rotation of shear-wave seismic data consists of two steps: finding the rotation parameters and actually applying the rotation. The rotation parameters are usually determined by rotation scanning, which is done by applying rotation for a range of parameters and picking the best parameters according to a certain criterion. The selected parameters are then used to rotate the data.

4.2.1 The principle of rotation of multisource multireceiver shear-wave data

Shown in Figure 4-1 is a plan view of an MSMR surface line for the situation where vertical shear-wave splitting is assumed to occur. Each wave generated by a shear-wave source whose polarization does not coincide with the natural coordinate axes will split into a fast and a slow wave (Crampin, 1981; Thomsen, 1988). The S_1 direction is the polarization direction of the shear waves travelling at the faster speed, β_1, while S_2

taken to be perpendicular to S_1, is the polarization direction of the shear waves travelling at the slower speed, β_2.
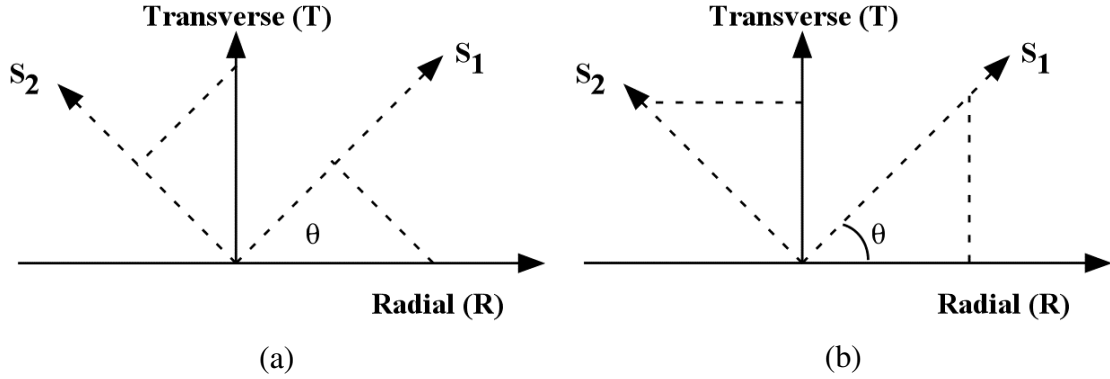

Figure 4-1. Illustration of the MSMR acquisition and shear-wave splitting; (a) shear waves generated by the radial and transverse sources split into fast (S_1) and slow (S_2) waves; (b) shear-waves polarized in the S_1 and S_2 directions will decompose into radial and transverse components.

Consider stacked data and assume that a conventional stack of a CMP gather forms a normal-incidence, multiple-free, noise-reduced trace. In actual MSMR acquisition, both the radial (SV) and transverse (SH) sources are applied and receivers along both the radial and transverse axes are deployed. The shear waves generated by the sources split into the fast and slow waves, which propagate vertically down and reflect independently from horizontal reflectors. The reflected fast and slow waves reach a receiver at different times and decompose into radial and transverse components. Therefore, the waves recorded by both the radial and transverse receivers contain both fast and slow waves superposed. Rotation of coordinate axes is carried out to separate the fast and slow waves.

Let $s_R(t)$ and $s_T(t)$ be the radial and transverse source amplitudes along acquisition coordinate axes, respectively. This can be expressed as the matrix:

$$S_a(t) = \begin{pmatrix} s_R(t) & 0 \\ 0 & s_T(t) \end{pmatrix}. \tag{4-1}$$

Both shear-wave sources will generate shear waves, each of which splits into shear waves polarized in the S_1 and S_2 directions (Figure 4-1(a)).

The relationship of splitting illustrated in Figure 4-1(a) can be expressed as matrix multiplication:

$$S_n(t) = \begin{pmatrix} \cos\theta & \sin\theta \\ -\sin\theta & \cos\theta \end{pmatrix} \begin{pmatrix} s_R & 0 \\ 0 & s_T \end{pmatrix} = \begin{pmatrix} s_R\cos\theta & s_T\sin\theta \\ -s_R\sin\theta & s_T\cos\theta \end{pmatrix}, \tag{4-2}$$

or

$$R(\theta)S_a(t) = S_n(t) \tag{4-3}$$

where θ is the rotation angle, which is defined as the angle between the polarization direction of the fast wave and the radial direction of the acquisition coordinate system (Figure 4-1(a)).

$R(\theta) = \begin{pmatrix} \cos\theta & \sin\theta \\ -\sin\theta & \cos\theta \end{pmatrix}$ is the vector rotation matrix and

$$R(-\theta) = R^{-1}(\theta) = R^T(\theta) = \begin{pmatrix} \cos\theta & -\sin\theta \\ \sin\theta & \cos\theta \end{pmatrix}. \tag{4-4}$$

$S_a(t) = \begin{pmatrix} s_R & 0 \\ 0 & s_T \end{pmatrix}$ is the source matrix in the acquisition coordinate system, and

$S_n(t) = \begin{pmatrix} s_R\cos\theta & s_T\sin\theta \\ -s_R\sin\theta & s_T\cos\theta \end{pmatrix}$ is the source matrix in the natural coordinate system,

each row of which represents the components that are polarized in the same direction, due to the splitting of shear waves generated by the radial and transverse sources, while each column of which represents components generated by the same source.

Similarly, if $U(t) = \begin{pmatrix} u_{11} & 0 \\ 0 & u_{22} \end{pmatrix}$ is a data matrix that would be recorded in the natural

coordinate system, where u_{11} and u_{22} are the reflected signals polarized in the S_1 and S_2 directions, respectively, then the data that would be recorded along acquisition coordinate system can be written as:

$$V(t) = R^{-1}(\theta)U(t) = \begin{pmatrix} u_{11}\cos\theta & -u_{22}\sin\theta \\ u_{11}\sin\theta & u_{22}\cos\theta \end{pmatrix}. \tag{4-5}$$

Based on the above discussion, we can write in the frequency domain that:

$$V(\omega) = R^{-1}(\theta)D(\omega)R(\theta)S_a(\omega) \tag{4-6}$$

where $D(\omega) = \begin{pmatrix} f_1(\omega)e^{-i\omega\delta_1} & 0 \\ 0 & f_2(\omega)e^{-i\omega\delta_2} \end{pmatrix}$ represents the traveltime-delay function of split

shear waves; δ_1 and δ_2 are the two-way traveltimes of the fast and slow waves, respectively, and $f_1(\omega)$ and $f_2(\omega)$ are the filter functions for the fast and slow wave propagation, respectively, which can account for the geometric spreading, attenuation, reflection coefficients, etc.

After rotation, we would like to have arrived at a data matrix that would have been generated by deploying both the sources and receivers along the natural coordinate axes; i.e., the output data matrix of the rotation should be:

$$W(\omega) = D(\omega)S_a(\omega) = D(\omega)R^{-1}(\theta)D^{-1}(\omega)R(\theta)V(\omega) \tag{4-7}$$

If $f_1(\omega) = f_2(\omega)$, equation (4-7) can be written as:

$$W(\omega) = \begin{pmatrix} w_{11} & w_{12} \\ w_{21} & w_{22} \end{pmatrix} =$$

$$\begin{pmatrix} \cos^2\theta + \sin^2\theta\, e^{+i\omega\Delta} & \sin\theta\cos\theta - \sin\theta\cos\theta\, e^{+iw\Delta} \\ \sin\theta\cos\theta\, e^{-i\omega\Delta} - \sin\theta\cos\theta & \sin^2\theta\, e^{-i\omega\Delta} + \cos^2\theta \end{pmatrix} \bullet \begin{pmatrix} v_{RR} & v_{RT} \\ v_{TR} & v_{TT} \end{pmatrix} \quad (4\text{-}8)$$

where, in symbols w_{ij} and v_{ij}, i represents the receiver direction, j represents the source direction, and $\Delta = 2_Z\left(\dfrac{1}{\beta_2} - \dfrac{1}{\beta_1}\right)$ is the time lag between the fast and slow waves. Multiplication by $e^{i\omega\Delta}$ or $e^{-i\omega\Delta}$ in the frequency domain is equivalent to a time shift of Δ or $-\Delta$, respectively, in the time domain.

According to equation (4-8), if we could determine the angle between the direction of the polarization of the fast shear wave and the radial direction, rotation angle, θ, and the time lag between the fast and slow waves, Δ, we can rotate the acquisition data matrix V into W to separate the fast and slow shear waves. These two parameters can be determined by scanning.

Note that in the rotation algorithm described above, it is not necessary to assume that the two wavelets of the radial and transverse sources be identical.

4.2.2 Scanning for the rotation parameters, θ and Δ

For most rotation algorithms, the critical part is to find the correct rotation parameters. A correct rotation should zero out or minimize the energy of the off-diagonal data elements in the data matrix. Alford's rotation algorithm uses only one parameter, θ, the rotation angle, which is estimated by computing the energy, or error norm, of the off-diagonal data elements (Alford, 1986; Zhang 1995). My algorithm uses two parameters: the rotation angle and the time lag. Therefore, it places more constraints on the determination of the rotation parameters.

In order to determine the rotation parameters, the input data matrix is rotated through a range of angles, θ, and time lags, Δ, and the norms of the off-diagonal elements of the rotated data matrix are computed, that is:

$$\left\| E_{ij}(\theta, \Delta, t) \right\|_p = \left(\sum_{k=0}^{N-1} \left| w_{ij}(\theta, \Delta, t + k\Delta t) \right|^p \right)^{\frac{1}{p}}, \quad i \neq j \qquad (4\text{-}9)$$

where N is the number of samples in the scanning window and p is a positive value. Then we sum the norms of the off-diagonal elements. If the θ and Δ are optimal, the sum of the error norms will reach a minimum. Usually, using different values of p will produce somewhat different error-norm contours. The optimal value of p can be found by testing.

An alternative measurement of error norm for scanning the parameters, θ and Δ, is:

$$\left\| E(\theta, \Delta, t) \right\|_p = \left(\sum_{k=0}^{N-1} \left(\left| w_{12}(\theta, \Delta, t + k\Delta t) \right|^p + \left| w_{21}(\theta, \Delta, t + k\Delta t) \right|^p \right) \right)^{-1}. \qquad (4\text{-}10)$$

The error norms computed can be plotted in the form of contours. In the following section, we shall see that the error norm represented by equation (4-10) can sometimes produce a scanning-contour pattern that is sharper than that obtained from equation (4-9). Note that when the rotation parameters are optimal, the error norm computed from equation (4-10) reaches a maximum, rather than a minimum, as is the case for equation (4-9). One may use both equations to pick the best estimates of the scanning parameters.

4.2.3 Alford's rotation algorithm

Alford (1986) presented an algorithm for the rotation of MSMR shear-wave data. Beginning with a matrix equation describing 1-D wave propagation (e.g. zero-offset reflection) in the situation where two orthogonal shear-wave sources are applied along the natural coordinate axes, he derived a matrix equation for the situation where the sources are oriented parallel to the acquisition coordinate axes, by rotating them counterclockwise through an angle θ. He then obtained a matrix equation relating the

shear-wave data recorded by the acquisition system with what would be recorded in the natural coordinate system:

$$W = R(\theta)VR^T(\theta) \tag{4-11}$$

or

$$\begin{pmatrix} w_{11} & w_{12} \\ \\ w_{21} & w_{22} \end{pmatrix} = \begin{pmatrix} v_{RR}\cos^2\theta + v_{TT}\sin^2\theta & v_{RT}\cos^2\theta - v_{TR}\sin^2\theta \\ + (v_{TR}+v_{RT})0.5\sin 2\theta & + (v_{TT}-v_{RR})0.5\sin 2\theta \\ \\ v_{TR}\cos^2\theta - v_{RT}\sin^2\theta & v_{TT}\cos^2\theta + v_{RR}\sin^2\theta \\ + (v_{TT}-v_{RR})0.5\sin 2\theta & - (v_{TR}-v_{RT})0.5\sin 2\theta \end{pmatrix} \tag{4-12}$$

where V is the data matrix recorded in the acquisition coordinate system, W is the data matrix after rotation into the natural coordinate system, θ is the rotation angle (Figure 4-1), and $R(\theta)$ is the rotation matrix.

Because the off-diagonal elements equal zero in the natural coordinate system, from equation (4-12), it is readily proved that:

$$v_{TR} = v_{RT} . \tag{4-13}$$

According to the shear-wave splitting mechanism expressed by equations (4-2) and (4-5), one can write:

$$v_{TR} = S_R(t-\delta_1)* f_1(t)\cos\theta\sin\theta - S_R(t-\delta_2)* f_2(t)\cos\theta\sin\theta \tag{4-14}$$

$$v_{RT} = S_T(t-\delta_1)* f_1(t)\cos\theta\sin\theta - S_T(t-\delta_2)* f_2(t)\cos\theta\sin\theta \tag{4-15}$$

where $f_1(t)$ and $f_2(t)$ are the filter functions for the fast and slow wave propagation, which account for the geometric spreading, attenuation, reflection coefficient, etc. And the symbol $*$ represents the convolution operator

Assuming that $f_1(t)$ and $f_2(t)$ are the same, we should have:

$$S_R(t) = S_T(t) \qquad\qquad\qquad (4\text{-}16)$$

According to equation (4-16), we know that the two shear-wave sources must have the same wavelet signatures, in order for the Alford's (1986) rotation algorithm to work properly for the MSMR case, while my rotation algorithm does not need this assumption.

4-3 Synthetic data tests

To test the rotation algorithm discussed in section 4-2, MSMR shear-wave data matrices are created. Each data matrix consists of four data elements. In a data matrix, the first row contains the radial components and second row the transverse components. The first column contains the components generated by the radial source and the second column the components generated by the transverse source. Each data matrix will be rotated by both my rotation algorithm and Alford's algorithm to compare the robustness. Parameters scanning results using both equations (4-9) and (4-10) will be presented. The contours obtained by equation (4-10) actually show maximum while those obtained using equation (4-9) show minimum of error norms.
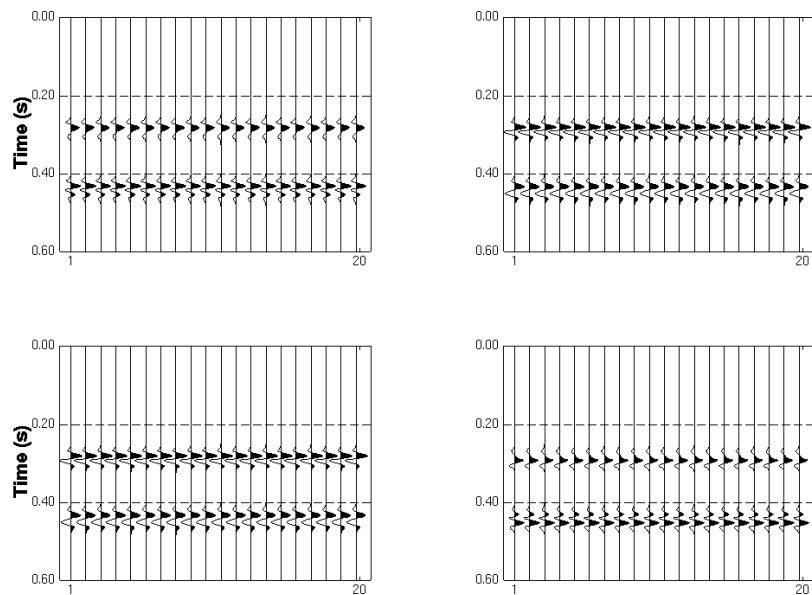
(a)
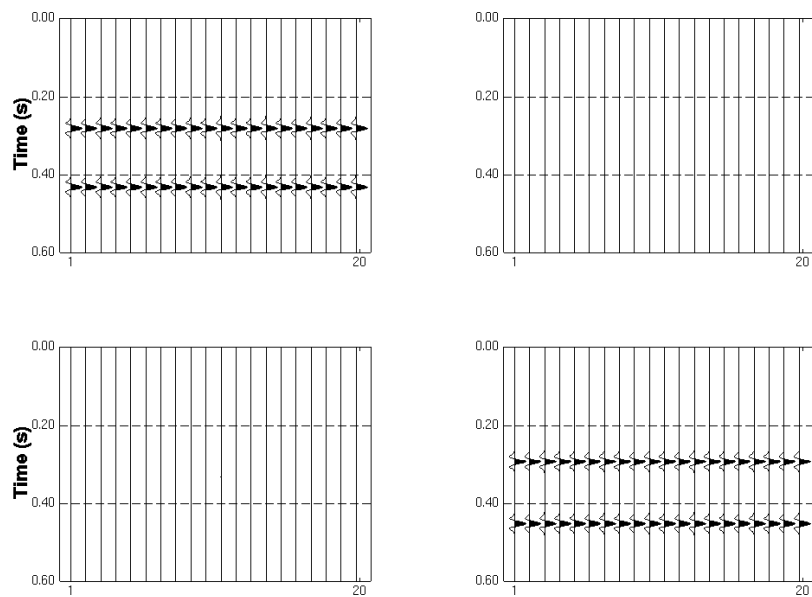
(b)
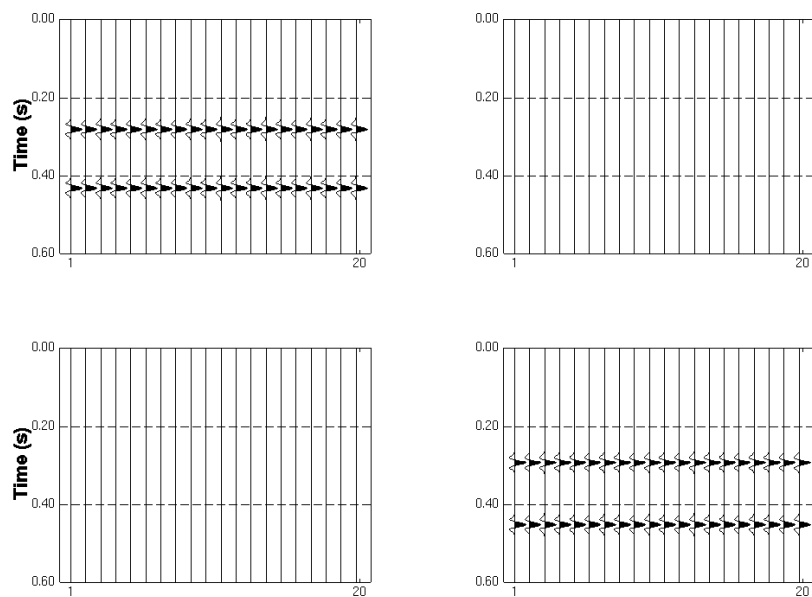
(c)

Figure 4-2. Synthetic data rotation showing (a) matrix before rotation of data generated by sources with the same wavelet signature; (b) data matrix rotated by my algorithm; (c) data matrix rotated by Alford's algorithm.

Figure 4-2(a) is an input data matrix generated by two sources with exactly the same wavelet. Figure 4-2(b) is the rotation result by my algorithm, while Figure 4-2(c) is the result by Alford's algorithm. Both methods work well when the two sources are the same. For rotation tests on synthetic data, only one CDP is created and repeated 20 times for the purpose of display.

Shown in Figure 4-3 is another synthetic data rotation test with input data matrix (Figure 4-3(a)) generated by sources with wavelets of different dominant frequencies and amplitudes. My algorithm completely removes the off-diagonal energy (Figure 4-3 (b)), while Alford's algorithm leaves significant energy on the off-diagonal elements (Figure 4-3(c)) because it requires that the wavelets of the two sources be the same.
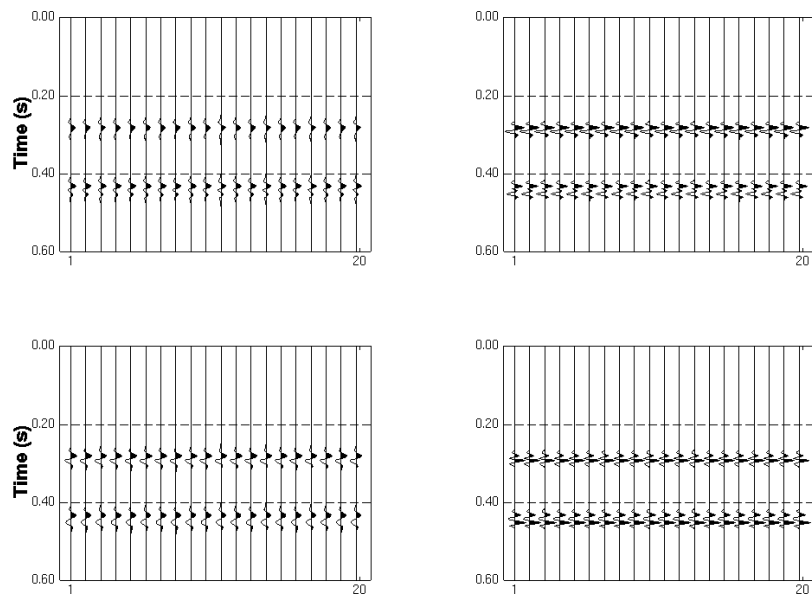
(a)
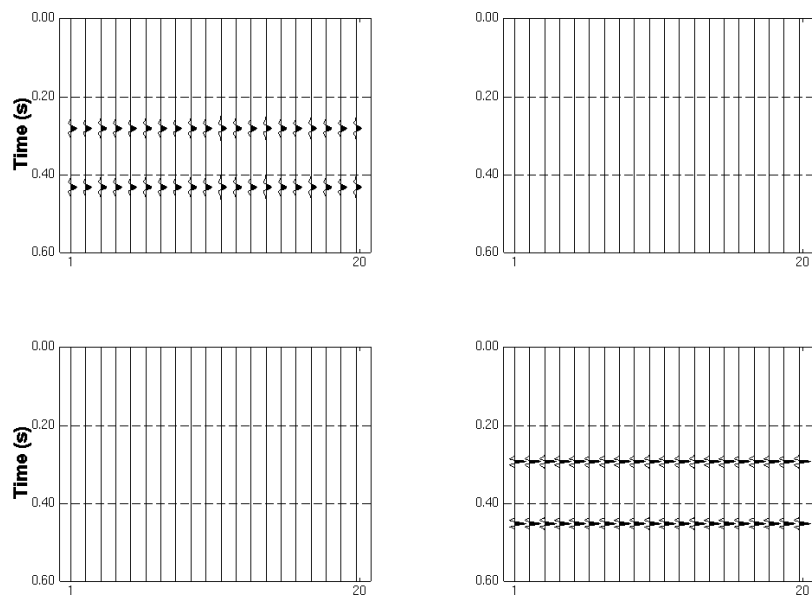
(b)
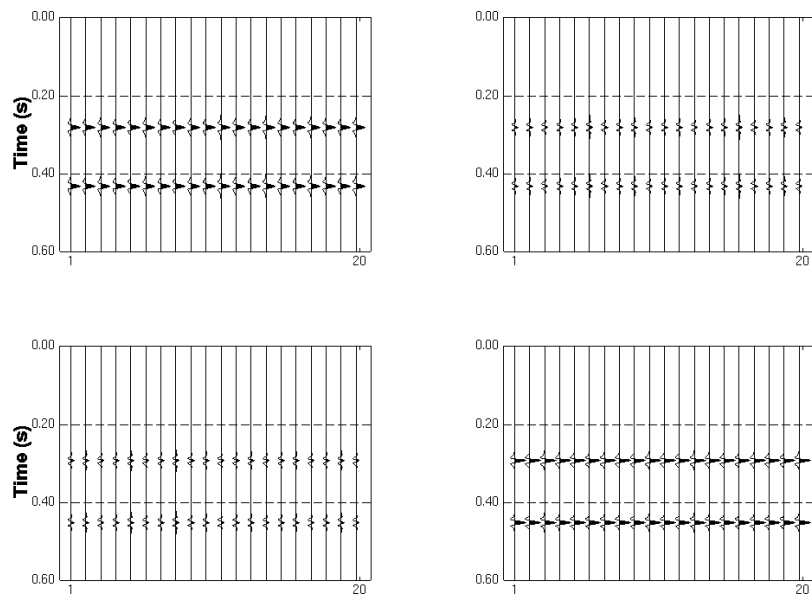
(c)

Figure 4-3. Synthetic data rotation showing (a) matrix before rotation of data generated by sources with wavelets different in dominant frequency and amplitude; (b) data matrix rotated by my algorithm; (c) data matrix rotated by Alford's algorithm.

Figure 4-4 shows a rotation test with band-limited random noise added to the input data matrix, which is generated by sources with exactly the same wavelet signatures. The mean amplitude of the noise is 0.05 times that of the signal. Figure 4-4(a) is the input data matrix, while Figure 4-4(b) is the rotation result by my algorithm and Figure 4-4(c) the rotation result by Alford's algorithm. It turned out that both methods work well for noisy data.
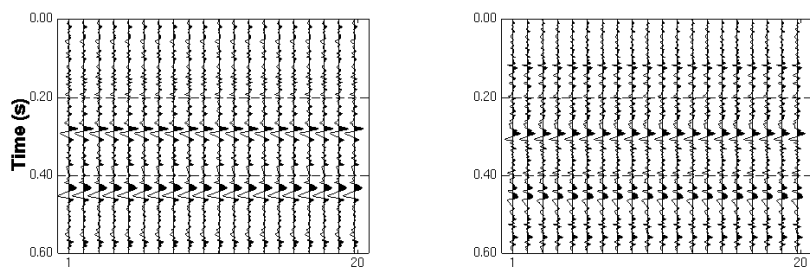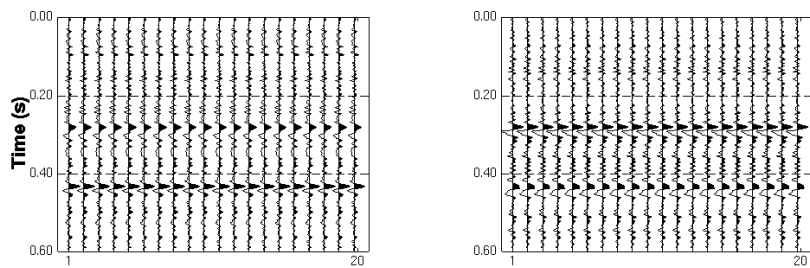
(a)
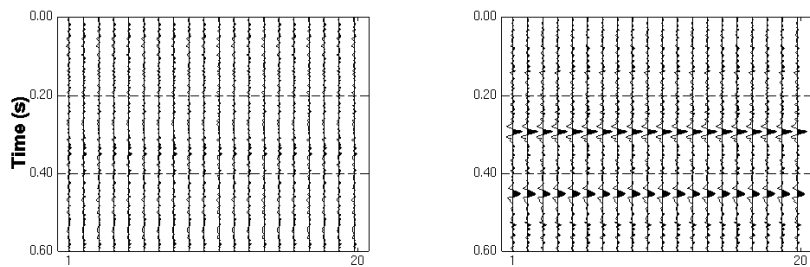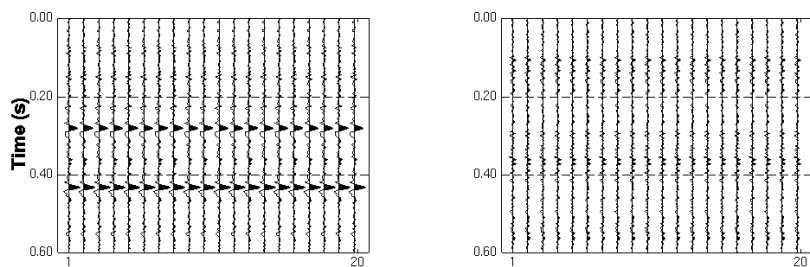
(b)
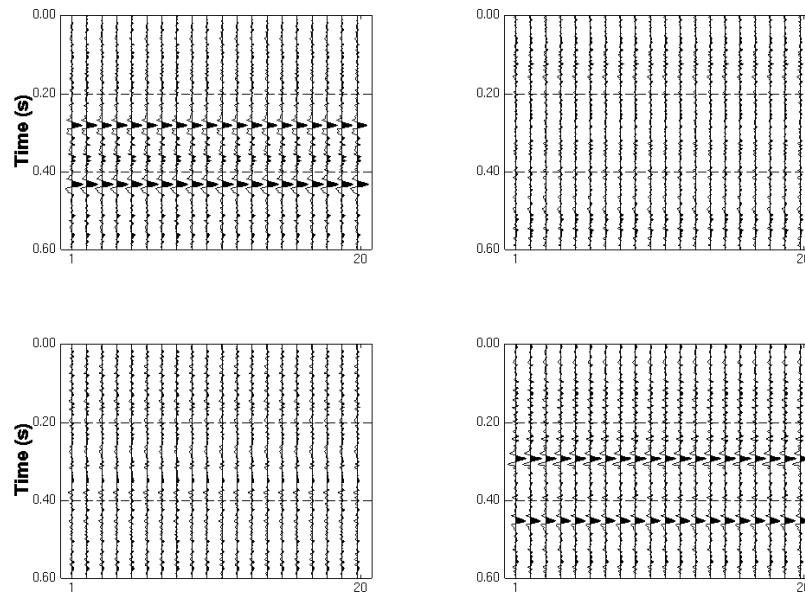
(c)

Figure 4-4. Rotation of synthetic data with band-limited random noise added to the input data matrix. The mean amplitude of noise is 0.05 times that of the signal; (a) input data matrix before rotation; (b) data matrix rotated by my algorithm and (c) data matrix rotated by Alford's algorithm.

Figure 4-5 shows results of scanning over the parameters θ and Δ (rotation angle and time lag) on the dataset of Figure 4-2, which is created with identical wavelets and is noise free. The scanning is performed at regular time steps and the sum of norms of off-diagonal elements of the rotated data matrix is displayed in contour form, which can be used to pick the desired parameters. Figures 4-5(a) and 4-5(c) demonstrate norm minima of good resolution: there are reflecting layers at these scanning times. And the parameters picked are exactly the same as those used to generate the data. As the scanning time moves away from a time at which there is a reflector, the norm minimum fades out and no parameters can be picked; as illustrated by Figures 4-5(b) and 4-5(d).

(a)   (b)

(c)   (d)
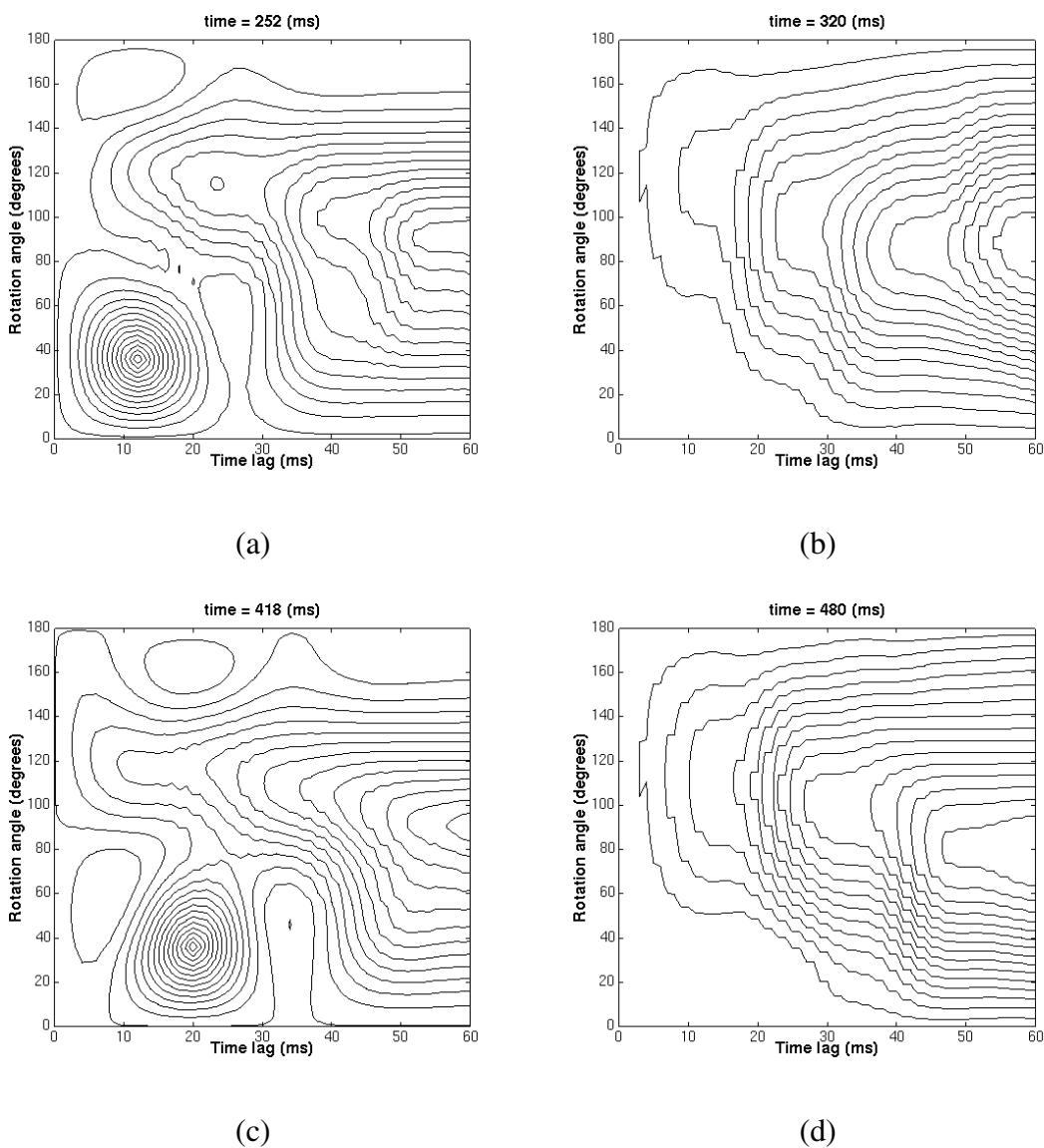
Figure 4-5. Scanning of rotation parameters, θ and Δ, on synthetic data at different reflection times.

The rotation scanning shown in Figure 4-5 is an ideal case in that the data contain no noise. We can actually expect all kinds of noise in field data processing. Figure 4-6 compares scanning results with and without noise. Figure 4-6(a) shows the result without noise, while Figure 4-6(b) shows the result at the same scanning time with noise added, where the mean amplitude of the noise is 0.05 times that of the signal. The norm

minimum is still clear enough, but with increased noise, the present scanning criterion does not give good resolution.
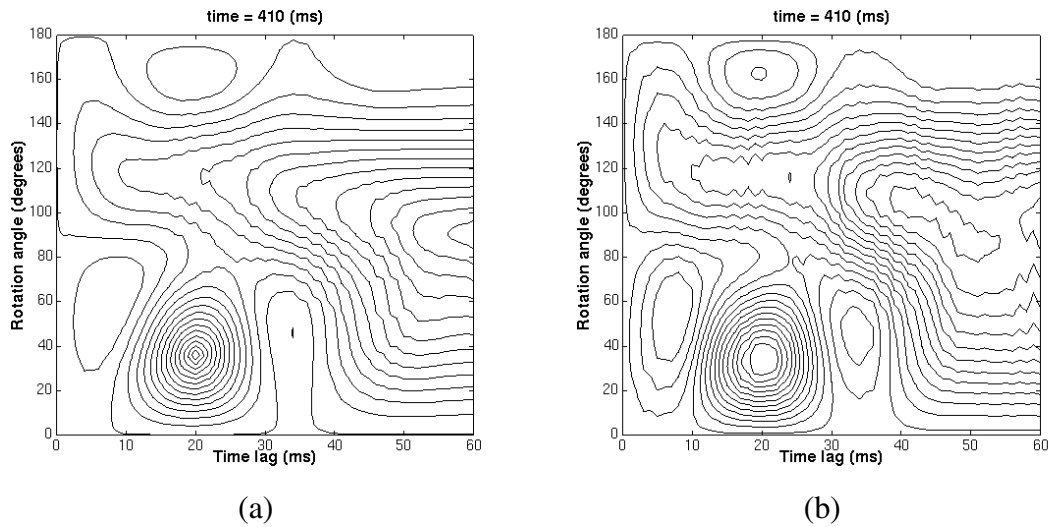
Figure 4-6. Scanning of rotation parameters, θ and Δ, on synthetic data at reflection time of 410 ms; (a) scanning without noise; (b) scanning with noise added to input data matrix; the mean amplitude of noise is 0.05 times of that of the signal.

Figure 4-7 shows the scanning contours using the error norm represented by equation (4-10). The input data are the same as in Figure 4-6. There is only one very sharp maximum in the contours, which shows the correct parameters. This type of norm is more robust in the presence of noise and could be preferred for field data.
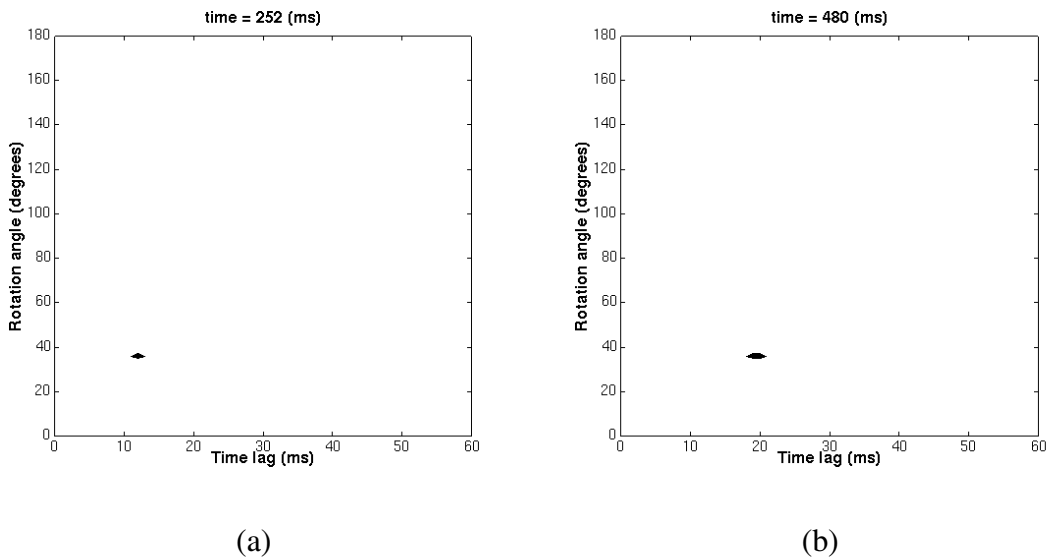
Figure 4-7. Scanning of rotation parameters, θ and Δ, on synthetic data using the error norm represented by equation (4-10); (a) at 252 ms; (b) at 480 ms.

An example of rotation of a 4-component data set generated by the pseudo-spectral numerical modelling is shown in Figure 4-8. Because we want to create stacked data for an azimuthally anisotropic medium, a source force is placed at each grid point along the line $x_3 = 25$ grid intervals and a receiver is placed at each grid point along the line $x_3 = 125$. Wavefields are simulated for sources polarized both in the x_1 and x_3 directions. The sources are different in terms of both amplitude and dominant frequency. Figure 4-8(a) is the input data matrix and Figure 4-8(b) is the resulting rotated data matrix by my algorithm. The off-diagonal energy is clearly removed and the fast and slow shear waves are separated.

(a)

(b)
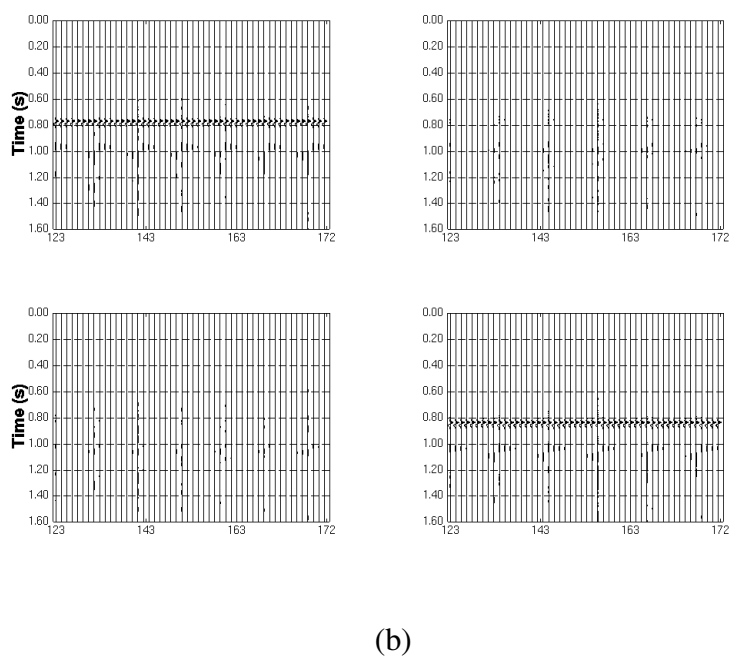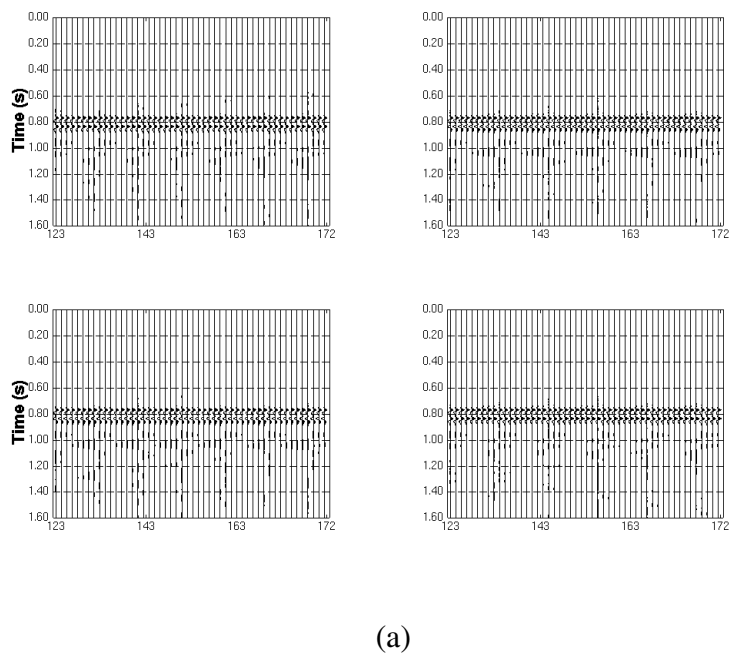
Figure 4-8. Four-component rotation of the synthetic data generated by pseudo-spectral numerical modelling; (a) data matrix before rotation; (b) data matrix after rotation.

Figure 4-9 shows the results of parameter scanning for the data used in Figure 4-8, at the traveltime of 800 ms on CMP 128. The values of θ and Δ are $45°$ and 68 ms, respectively, which can be verified by simple computations with the method for computing group velocities discussed in Chapter 2. Figure 4-9(a) is the result using the norm represented by equation (4-9) and Figure 4-9(b) is the result using the norm represented by equation (4-10). Figure 4-9(b) shows a much sharper maximum, but not necessarily higher resolution. Nevertheless, both kinds of norms may be computed and compared to ease the picking of rotation parameters in practical applications.

(a)   (b)
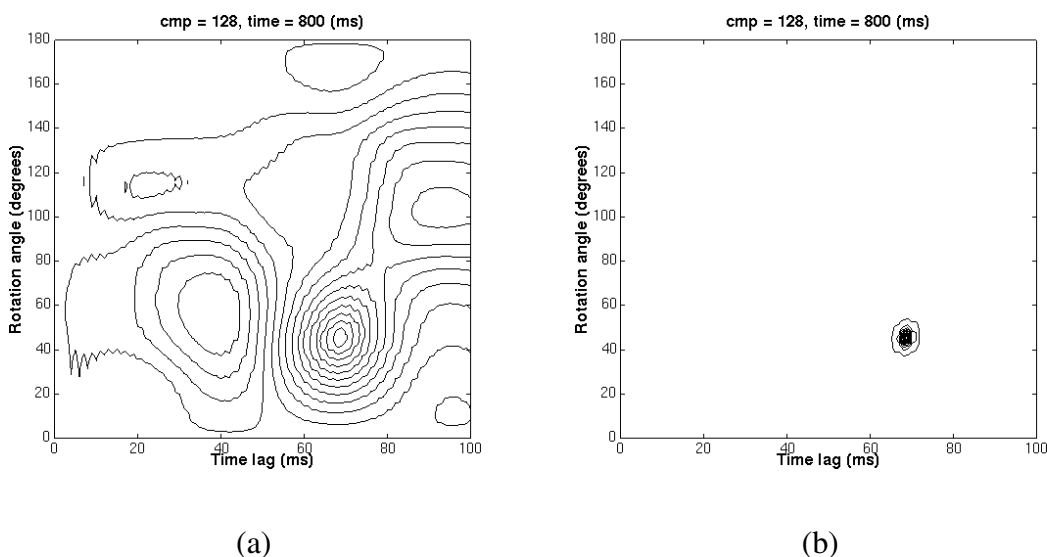
Figure 4-9. Scanning of rotation parameters, θ and Δ, at traveltime 800 ms on CMP 128 of dataset in Figure 4-8, which is created by pseudo-spectral numerical modelling.

4-4 Field data example

Figure 4-10 shows two examples of parameter scanning on field data. Because of the noise and the deviation of real situations from the theoretical assumptions, such as the fact that a CMP stacked section does not exactly represent zero-offset data, we have mixed scanning results. We see fairly good resolution in the scanning case shown by

Figure 4-10(a) and poorer resolution in the case of Figure 4-10(b). It turns out that at the traveltimes where there are strong reflections and high signal-to-noise (S/N) ratio, the scanning results are good. In the rotation of real data, other information about the natural polarization direction is usually needed.

(a)   (b)
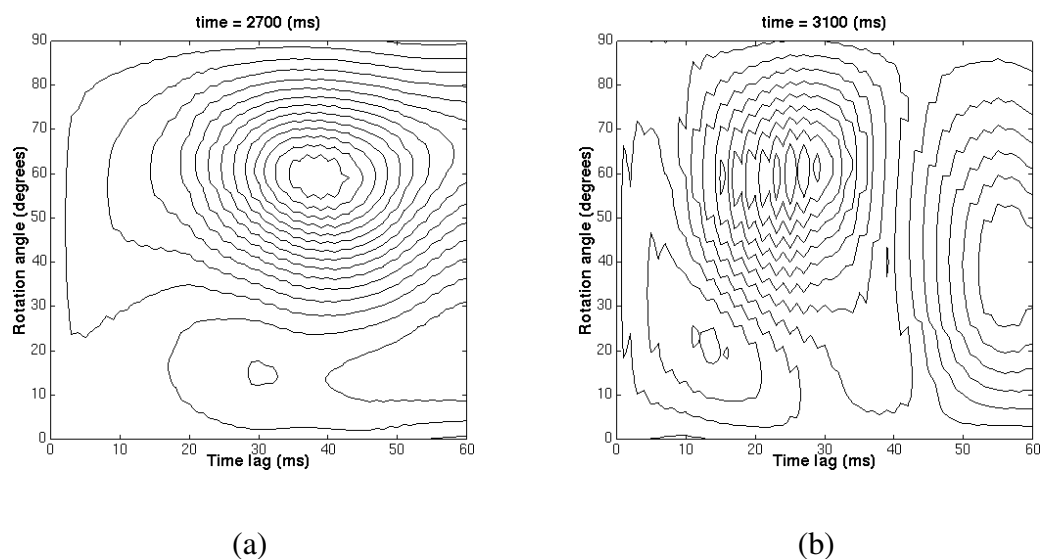
Figure 4-10. Scanning on field data; (a) good minimum resolution at a traveltime where reflections are strong and S/N ratio is high; (b) poor resolution at a traveltime where reflections are weak and S/N ratio is low.

Figure 4-11(a) is a field data matrix before rotation from the Olds area, Alberta. The off-diagonal data elements demonstrate strong signal energy, which indicates that there could be azimuthal anisotropy. Figure 4-11(b) is the rotated result, where the off-diagonal signal energy has been greatly reduced and diagonal signal energy is enhanced. Also, the fast and slow shear waves have been separated.
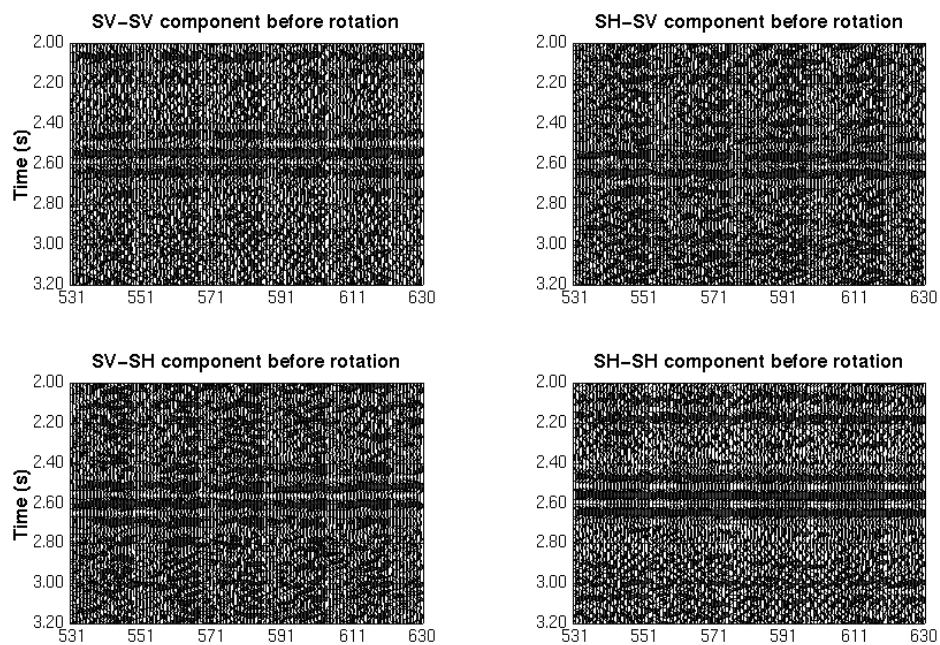
(a)
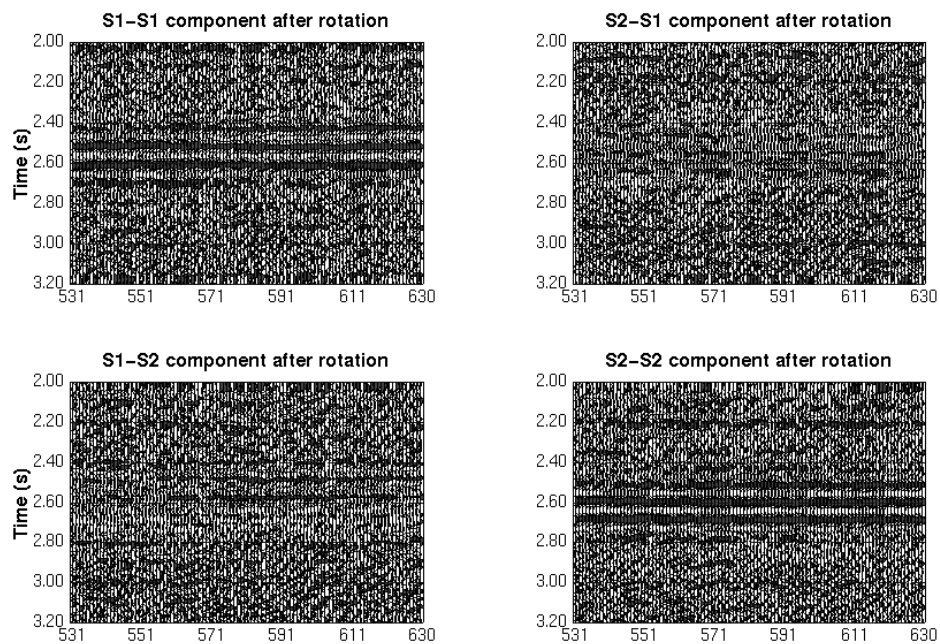
(b)

Figure 4-11. Field data rotation; (a) data matrix before rotation; (b) data matrix after rotation.

Figure 4-12(a) shows the input diagonal data elements side by side, while Figure 4-12(b) displays the fast and slow waves in the same way as the input data are shown to show the time lag between them. Rotation will facilitate the interpretation by separating the fast and slow shear waves, thus clarifying the shear wave sections, and also by giving information about fractures and the cause of anisotropy.

(a)

(b)
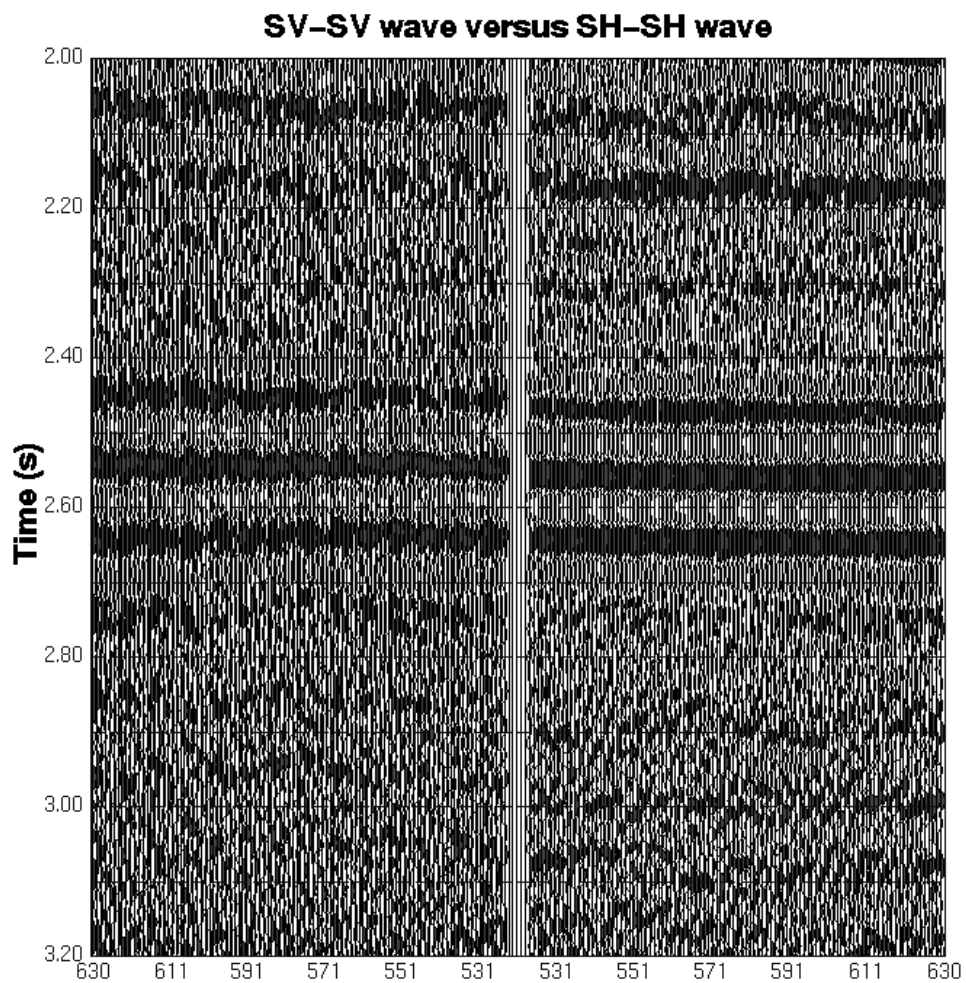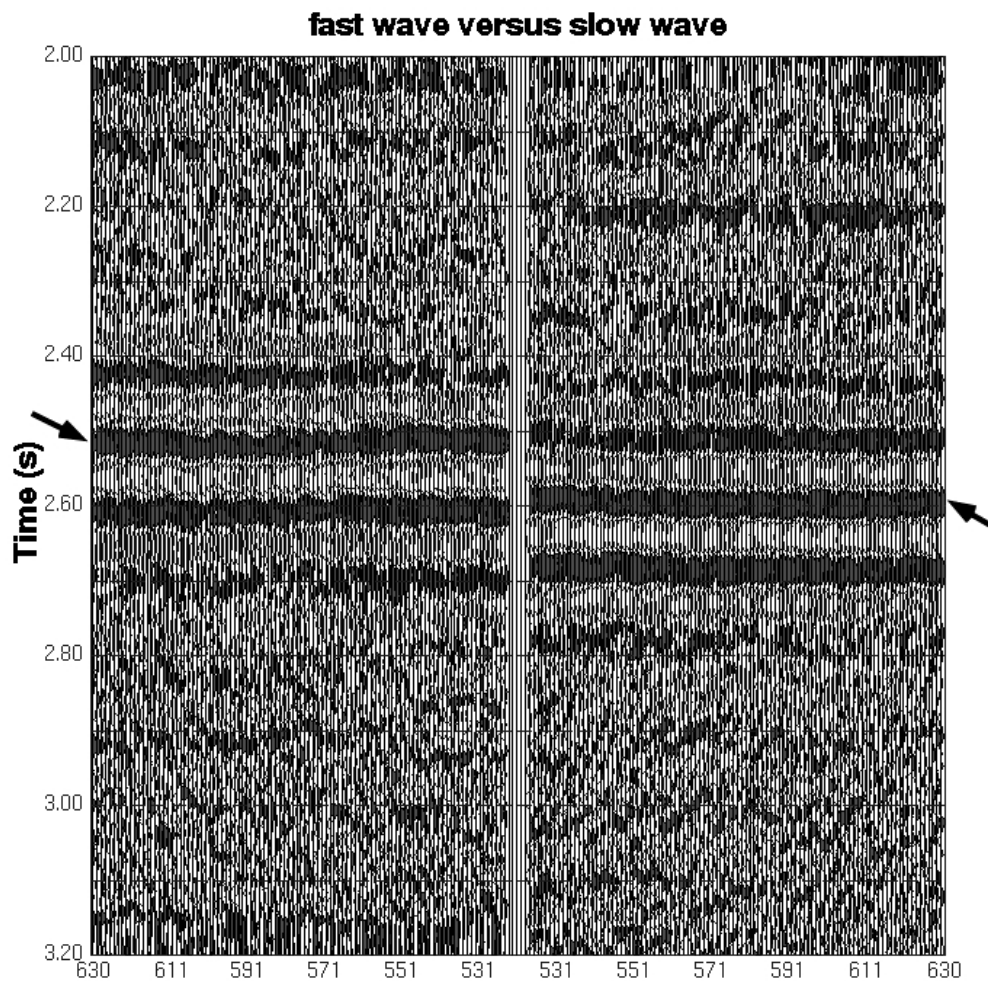
Figure 4-12. Field data rotation; (a) diagonal data elements before rotation; (b) separated fast and slow waves after rotation.

4-5 Summary

A new algorithm is presented based on a derivation that better describes the azimuthal anisotropy problem. By rotation scanning, two parameters, rotation angle and time lag between the fast and slow waves, can be determined, while Alford's method can

only scan for the rotation angle. The new algorithm can better deal with the data generated by two sources with different wavelet signatures, as opposed to Alford's rotation algorithm, which assumes identical source signatures. It is also robust in the presence of relatively strong noise. Synthetic data tests and one field data example illustrate the promise of the method for general application.

Chapter 5:   Rotation of SSMR shear-wave seismic data

5.1 Introduction

For the azimuthal anisotropy caused by vertical fractures or cracks, the rotation angle and time lag between the fast and slow shear waves can be obtained by the rotation scanning of MSMR shear-wave data. But it is usually very expensive to acquire MSMR data. A more economically practical alternative is to use a single shear-wave source, or simply a P-wave source that produces converted shear waves. Therefore, rotation of single-source multireceiver (SSMR) shear-wave data is of practical interest.

It is well known that part of a P wave's energy will be converted to shear-wave energy upon incidence at a reflecting interface. If the medium above the reflector is azimuthally anisotropic, the converted shear wave will, in general, split into a fast and a slow shear wave in travelling back from the conversion point to the surface. It would seem that the converted shear wave is generated by a single radial shear-wave source, since the incident P wave has no transverse polarization component. Rotation is needed to separate the fast and slow shear waves and to find the rotation angle and time lag for the purpose of delineating the fractures and separate the fast and slow waves.

5.2 Principles of parameter scanning and rotation

SSMR (or P-SV) acquisition can be viewed as a special case of MSMR acquisition. Figure 4-1 can be used to explain the splitting of shear waves generated by a single radial source, or P-SV source, $S_R(t)$.

$S_R(t)$ will split into fast and slow waves, $S_1(t)$ and $S_2(t)$, polarized in the S_1 and S_2 direction, respectively (Figure 4-1(a)):

$$S_1(t) = S_R(t)\cos\theta \qquad (5\text{-}1\text{-}1)$$

$$S_2(t) = -S_R(t-\Delta)\sin\theta \qquad (5\text{-}1\text{-}2)$$

where, θ is the rotation angle and Δ is the time lag.

The wavefields recorded by the radial and transverse receivers would be:

$$V(t) = \begin{pmatrix} v_1(t) \\ v_2(t) \end{pmatrix} = \begin{pmatrix} \cos\theta & -\sin\theta \\ \sin\theta & \cos\theta \end{pmatrix} \begin{pmatrix} S_1(t) \\ S_2(t) \end{pmatrix}. \qquad (5\text{-}2)$$

Therefore, we have:

$$v_1(t) = S_R(t)\cos^2\theta + S_R(t-\Delta)\sin^2\theta \qquad (5\text{-}3\text{-}1)$$

$$v_2(t) = S_R(t)\sin\theta\cos\theta - S_R(t-\Delta)\sin\theta\cos\theta. \qquad (5\text{-}3\text{-}2)$$

Transformed into the frequency domain, we obtain:

$$V_1(\omega)/S_R(\omega) = \cos^2\theta + \sin^2\theta e^{-i\omega\Delta} \qquad (5\text{-}4\text{-}1)$$

$$V_2(\omega)/S_R(\omega) = \sin\theta\cos\theta - \sin\theta\cos\theta e^{-i\omega\Delta}. \qquad (5\text{-}4\text{-}2)$$

From equation (5-4), we can get:

$$V_1(\omega)(1 - e^{-i\omega\Delta})\sin 2\theta = 2V_2(\omega)(\cos^2\theta + e^{-i\omega\Delta}\sin^2\theta) \qquad (5\text{-}5)$$

or in the time domain:

$$E(\theta,\Delta,t) = (v_1(t)\sin 2\theta - 2v_2(t)\cos^2\theta) - (v_1(t-\Delta)\sin 2\theta + 2v_2(t-\Delta)\sin^2\theta) = 0. \ (5\text{-}6)$$

Equation (5-6) can also be derived by observing single-source acquisition as a special case of multisource acquisition.

Using Equation (5-6) for a range of rotation angles, θ, and time lags, Δ, the error norm is computed from:

$$\|E(\theta, \Delta, t)\|_p = \left(\sum_{k=0}^{N-1} |E(\theta, \Delta, t + k\Delta t)|^p \right)^{\frac{1}{p}} \qquad (5\text{-}7)$$

or, alternatively, from:

$$\|E(\theta, \Delta, t)\|_p = \left(\sum_{k=0}^{N-1} |E(\theta, \Delta, t + k\Delta t)|^p \right)^{-1}. \qquad (5\text{-}8)$$

Plotted as contours versus rotation angle and time lag, the norms computed by equation (5-7) have a "normal" look, while those computed by equation (5-8) show only the very sharp maxima, which should correspond to the correct parameters when the S/N ratio is high. Therefore equation (5-8) is preferred for noisy data or at least can be used simultaneously with equation (5-7). It should be noticed that equation (5-7) gives minima while (5-8) produces maxima for optimal scanning parameters.

Once the rotation parameters are obtained, rotation can be performed to obtain the components of shear-wave data that would have been recorded, had the receivers been placed along the natural coordinate axes, with the single source still being polarized in the radial direction. This amounts to rotating the components of data recorded by the real receivers in the acquisition coordinate system counterclockwise into the natural coordinate system by an angle of θ:

$$\begin{pmatrix} S_1(t) \\ S_2(t) \end{pmatrix} = \begin{pmatrix} \cos\theta & \sin\theta \\ -\sin\theta & \cos\theta \end{pmatrix} \begin{pmatrix} v_1(t) \\ v_2(t) \end{pmatrix}. \qquad (5\text{-}9)$$

As equation (5-9) suggests, the actual rotation of SSMR shear-wave data needs only the rotation angle, but both rotation angle and time lag can be obtained by the scanning outlined above.

5-3 Harrison's rotation algorithm

Harrison's (1992) rotation algorithm for SSMR shear-wave data is based on the forward modelling of crosscorrelation or its odd part using the sum of autocorrelations, all of the rotated components. It was found that the sum of the autocorrelations of the rotated components should be equal or proportional to the autocorrelation of the shear-wave source wavelet, provided that the autocorrelation of noise is zero or the S/N ratio is very high.

The crosscorrelation, or its odd part, of the rotated components can be forward modelled by analytical equations derived by Harrison (1992). Also, it can be computed directly from the rotated data. Therefore, the so-called normalized prediction error energy for the total crosscorrelation, or its odd part, can be computed by integrating over the full range of trial rotation angle, $\tilde{\theta}$ (-90° to 90°) for each pair of true rotation angle, θ, and time lag, Δ. Error energy is computed for a range of rotation angle and time lag.

The major assumption (Harrison, 1992) is that the sum of the autocorrelations of the rotated components should be equal or proportional to the autocorrelation of the shear-wave source wavelet. This may be satisfied only when noise is random or S/N ratio is very high.

5-4 Synthetic data examples

Figure 5-1 shows a synthetic data example of SSMR shear-wave rotation. The input data set (Figure 5-1(a)) consists of the two components recorded from a radial source with noise added. The mean amplitude of the noise is 0.05 times that of the signal. Rotation is done using the algorithm represented by equation (5-9) with known rotation angle. The fast wave and slow wave are fully separated (Figure 5-1(b)). This also demonstrates that this single-source rotation algorithm works well for data with relatively strong noise.
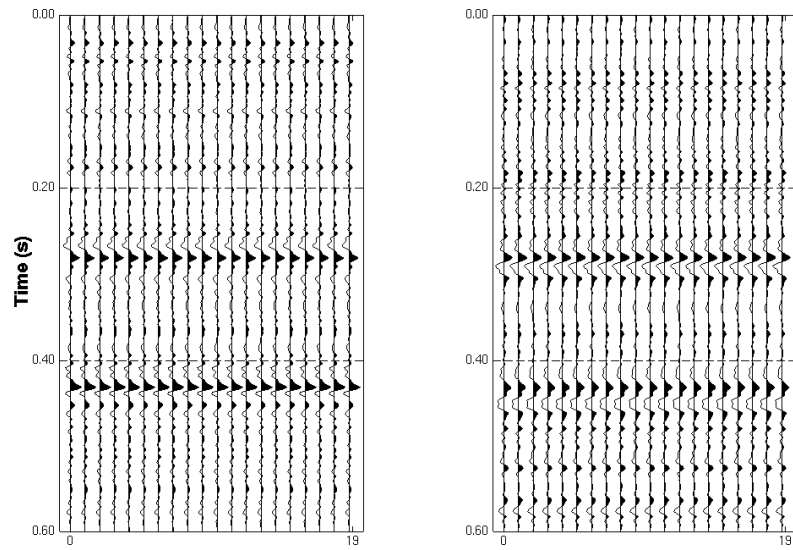
(a)
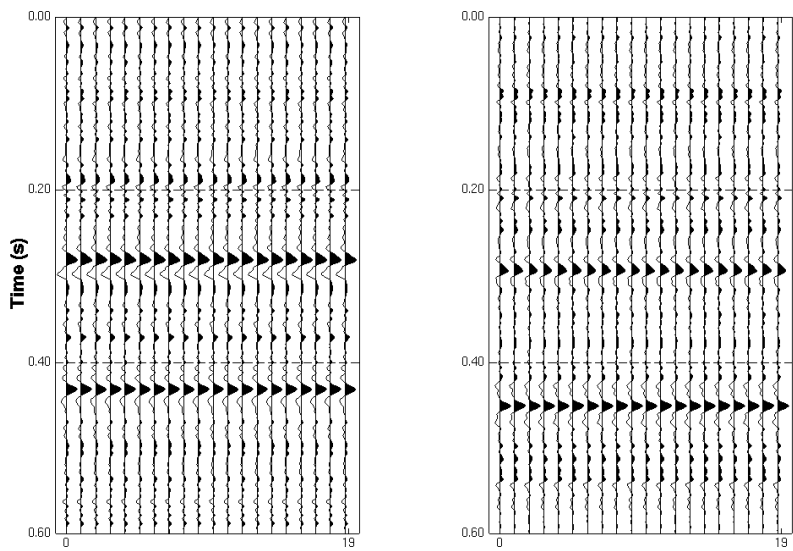
(b)

Figure 5-1. Synthetic data example of SSMR shear-wave rotation, radial component on the left and transverse component on right : (a) input data; (b) rotated output.
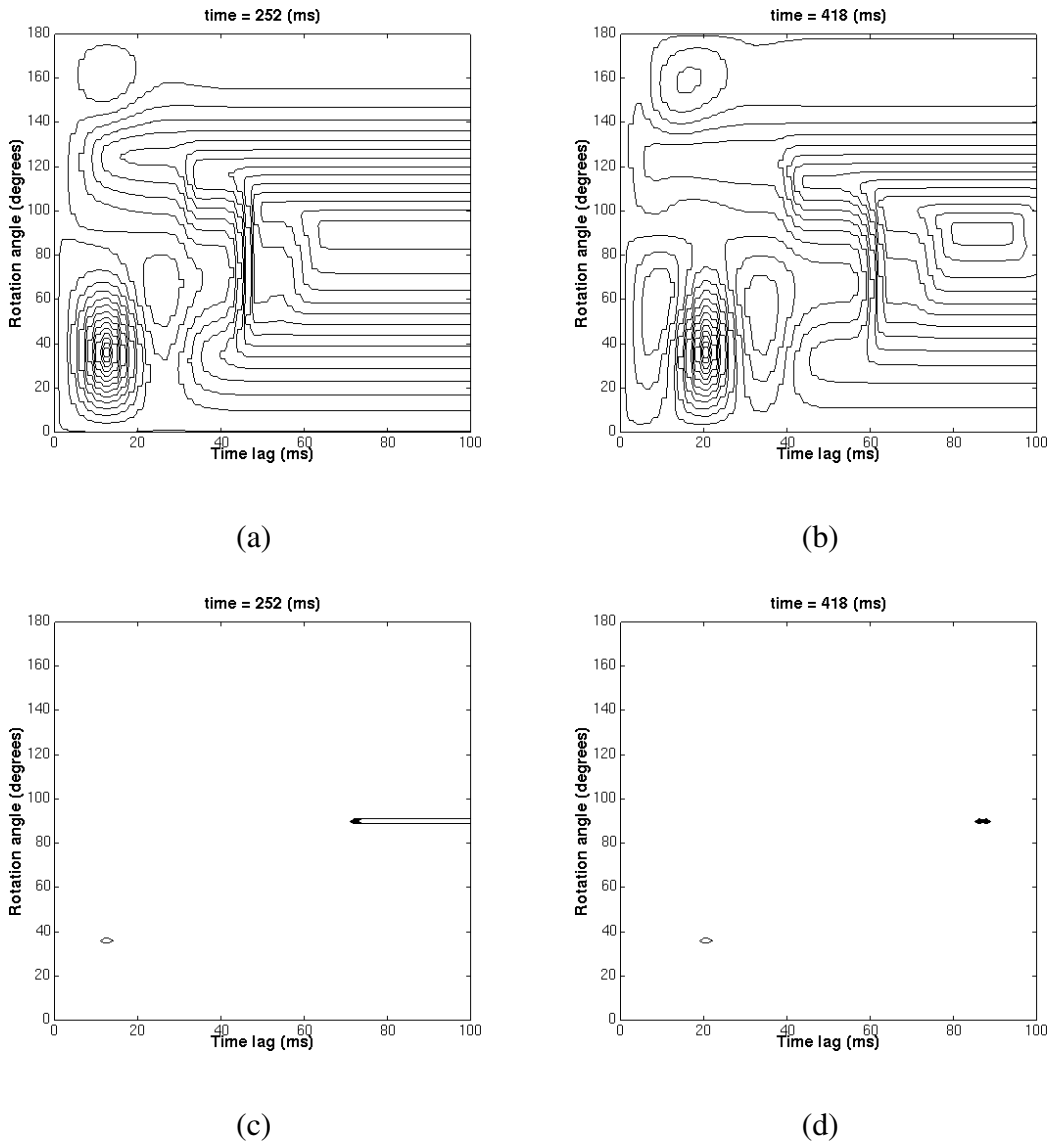
Figure 5-2. Scanning of rotation parameters: θ, rotation angle, and Δ, time lag: (a) and (b), which show the minimum, are the scanning results by the method represented by equation (5-7); (c) and (d), which show maximum, are the results by the method represented by equation (5-8). It is difficult to pick the parameters on (c) and (d) in this example.

Shown in Figure 5-2 is the parameter-scanning result for the SSMR shear-wave situation. By scanning the synthetic data, both the rotation angle, θ and the time lag, Δ,

can be determined. Notice that the method represented by equation (5-8) produces sharper contours. But in the case of Figure 5-2(c) or (d), it also includes other maxima, which are resulted from noise. This makes the picking of parameters no easier than by using the contours obtained from equation (5-7). Both equations may be used in order to get the best picking result in real data applications. The parameters obtained by scanning are the same as the parameters used for generating the input synthetic data.

In Figure 5-3, the synthetic shear-wave data generated by the pseudo-spectral method are used to test the rotation algorithm. The model is the same as the model used in Figure 4-8 of Chapter 4, but only the shear-wave data generated by the radial source are used. As shown in Figure 5-3, fast waves and slow waves are fully separated. The rotation result is comparable to the result by four-component rotation shown in Figure 4-8.
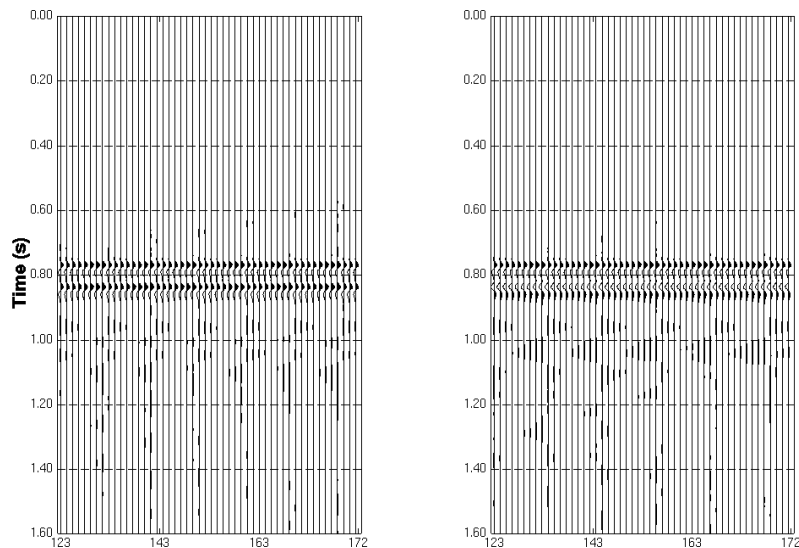
(a)
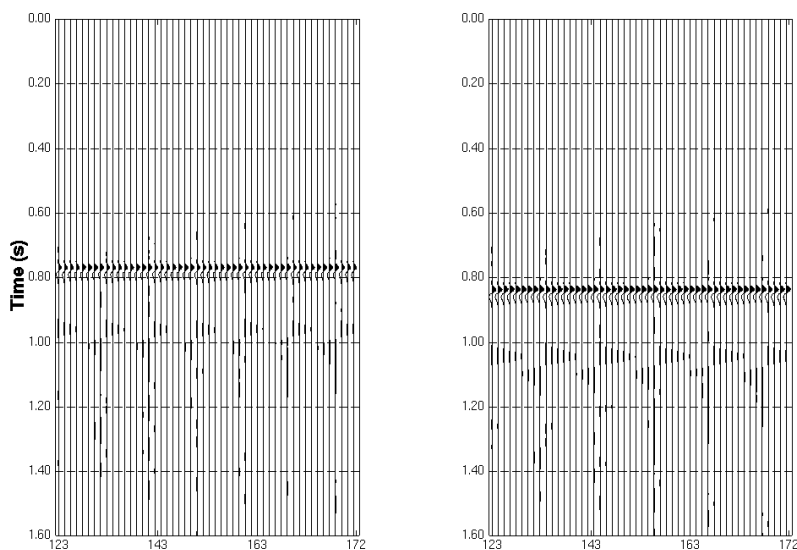
(b)

Figure 5-3. Rotation of single-source shear-wave data generated by pseudo-spectral method: (a) input data generated by radial source; (b) rotated output.

The rotation parameters used in Figure 5-3 are obtained by scanning as shown in Figure 5-4. Again the method represented by equation (5-8) produces sharper contour (Figure 5-4(b)) compared to the result by the method represented by equation (5-7) (Figure 5-4(a)). Scanning results by both methods may be used in picking the rotation parameters.

(a)   (b)
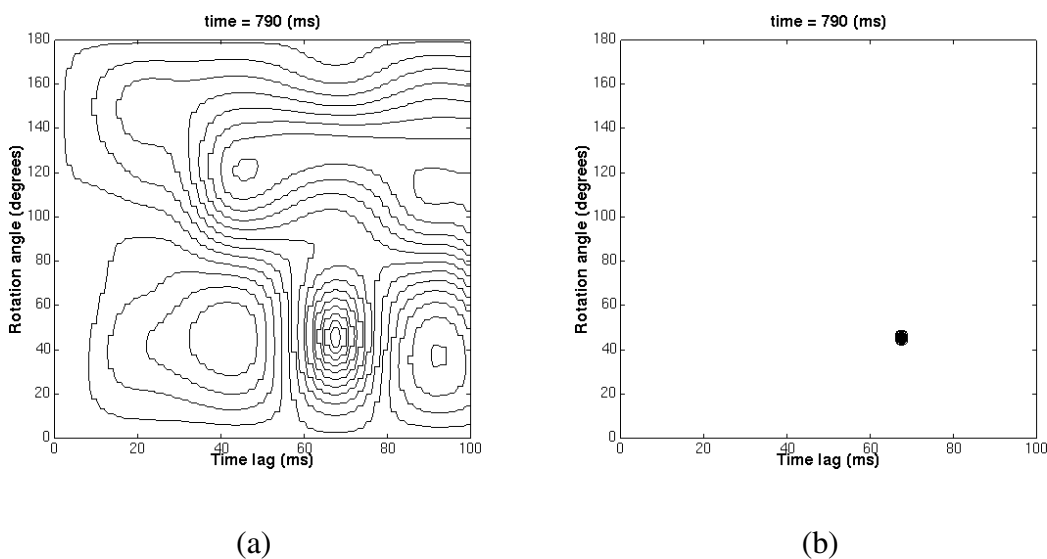
Figure 5-4. Rotation parameters scanning for the synthetic data generated by pseudo-spectral numerical modelling: (a) result by equation (5-7) (minimum); (b) result by equation (5-8) (maximum).

5.5 Summary

The algorithm for the rotation of the SSMR shear-wave data is simple but robust. It does not require any assumptions on the shear-wave signals of both source and receivers, while Harrison's method assumes that the sum of the autocorrelations of the rotated components is equal or proportional to that of the input shear signal, which may fail when there is strong coherent noise. The advantage of this scanning algorithm is that it produces two rotation parameters, rotation angle and time lag between the fast and slow shear waves. Synthetic data tests show that the parameter scanning is stable and accurate. It produces results that are as good as the four-component scanning results discussed in Chapter 4.

Chapter 6: Conclusions and Future work

6.1 Conclusions

Cracked media can be modelled with Hudson's theory by computing the stiffness tensor from crack density and the Lamé constants of the uncracked media. Within the range of weak anisotropy, the Thomsen anisotropy parameters, ε, δ and γ, and the phase and group velocities can be computed. Thus, properties of azimuthal anisotropy can be related directly to crack density.

The stiffness tensor computed with Hudson's theory is used in the numerical simulation of wave propagation in anisotropic media. The computation load of the anisotropic modelling is excessive. Therefore, the pseudo-spectral method is chosen to do the numerical modelling because of its relatively fast computation speed compared with other methods. It is accurate and suitable for inhomogeneous media. The pseudo-spectral method proves to be successful in modelling 2D anisotropic media and can be used to generate test data for evaluating rotation algorithms. The major problems of the pseudo-spectral method include wavenumber dispersion due to multiplication in the wavenumber domain and difficulty in achieving complete edge-effect elimination. Although 2D pseudo-spectral numerical modelling in anisotropic media is feasible, it is still impractical to run 3D simulation on a single Sun workstation.

New rotation algorithms for both the MSMR and SSMR shear-wave data are developed and tested on synthetic data and field data. The new algorithms prove to be successful and robust for noisy data. The rotation algorithm for MSMR data can deal with the case where the two sources have different wavelet signatures, while Alford's method requires identical wavelet signatures, which is rarely met in real data situations.

SSMR data rotation is of special interest for industry application because of the relatively low cost of acquiring SSMR shear-wave data (e.g. P-SV data). The algorithm for the SSMR case presented in the thesis is simple and robust compared with Harrison's

(1992) method, which assumes that the autocorrelation of the input traces is equal to that of the shear signal.

One of the key steps in the rotation of shear-wave data is to find the rotation parameters, the rotation angle and time lag between the fast and slow waves. The new algorithms provide a reliable mechanism to scan for these parameters.

6.2 Future work

Hudson's theory is useful for modelling cracked media. It could be used to model particular cracked media with e.g. inclusions of hydrocarbon or other fluids and compared with physical experiments on the corresponding cracked media. Similar comparisons have been reported by, e.g., Rathore et al. (1991) for cracked synthetic sandstones and by Rümpker et al. (1996) for an orthorhombic phenolic.

The edge-effect-elimination method and wavenumber dispersion phenomenon need to be investigated for the pseudo-spectral numerical simulation. It is also realistic and preferred to model azimuthally anisotropic media in 3D.

More work needs to be done on the rotation parameter-scanning scheme for the situation of noisy field data. This may consider the changes of anisotropy attributes with depth (layer stripping). The rotation algorithms could also be adapted to rotate pre-stack shear-wave data.

References

Alford, R. M., 1986, Shear data in the presence of azimuthal anisotropy: Dilley, Texas: 56th Internat. Mtg., Soc. Expl. Geophys., Expanded Abstracts, Session: s9.6.

Berryman, J.G., 1979, Long-wave elastic anisotropy in transversely isotropic media: Geophysics, 44, 896-917.

Carcione, J.M., 1990, Wave propagation in anisotropic linear viscoelastic media: Theory and simulated wavefields: Geophy. J. Int., 101, 739-750.

Cerjan, C., Kosloff, D., Kosloff, R. and Reshef, M., 1985, A nonreflecting boundary condition for discrete acoustic and elastic wave equations: Geophysics, 50, 705-708.

Cheadle, S.P., Brown, R.J., and Lawton, D.C., 1991, Orthorhombic anisotropy: A physical seismic modeling study: Geophysics, 56, 1603-1613.

Crampin, S, 1981, A review of wave motion in anisotropic and cracked elastic media: Wave motion, 3, 343-391.

Crampin, S., 1984, Effective anisotropic elastic constants for wave propagation through cracked solids: Geophys. J. R. astr. Soc., 76, 135-145.

Crampin, S. and Lovell, J.H., 1991, A decade of shear-wave splitting in the Earth's crust: what does it mean? what use can we make of it? and what should we do next? Geophys. J. Int., 107, 387-407.

Dong, Z. and McMechan, G.A., 1995, 3-D viscoelastic anisotropic modelling of data from a multicomponent, multi-azimuth seismic experiment in northeast Texas: Geophysics, 60, 1128-1138

Esmersoy, C., 1990, Split-shear wave inversion for fracture evaluation: 60th Internat. Mtg., Soc. Expl. Geophys., Expanded Abstracts, 1400-1403.

Faria, E.L. and Stoffa, P.L., 1994, Finite-difference modelling in transversely isotropic media: Geophysics, 59, 282-289.

Gazdag, J., 1981, Modeling of acoustic wave equation with transform methods: Geophysics, 46, 854-857.

Guest, W.S. and C.J. Thomson, 1993, Anisotropic reflection and transmission calculations with application to a crustal seismic survey from the east Greenland shelf: J. Geophy. Research, 98, 14,161-14,184.

Harrison, M.P., 1992, Processing of P-SV surface data: Anisotropy analysis, dip moveout, and migration: Ph.D thesis, The University of Calgary, Alberta, Canada.

Helbig, K., 1994, Foundations of anisotropy for exploration seismics: Oxford: Pergamon.

Hudson, J.A., 1981, Wave speeds and attenuation of elastic waves in material containing cracks, Geophys. J. R. astr. Soc., 64, 133-150.

Hudson, J. A., 1982, Overall properties of a cracked solid: Math. Proc. Camb. Phil. Soc., 88, 371-384.

Kosloff, D., Reshef, M. and Loewenthal, D., 1984, Elastic wave calculations by Fourier method: Bull. Seism. Soc. Am., 74, 875-891.

Kosloff, D. and Carcione, J.M., 1989, Three-dimentional wave propagation simulation in elastic-anisotropic media: 59th Internat. Mtg., Soc. Expl. Geophys., Expanded Abstracts, 1016-1018.

Lou, M. and Rial, J.A., 1995, Modelling elastic wave propagation in inhomogeneous anisotropic media by the pseudo spectral method: Geophys. J. Int., 120, 60-72.

Lynn, H.B., Simon, K.M., Bates, C.R., Layman, M. and Schneider, R., 1995, Seismic characterization of a naturally fractured gas reservoir: 59th Internat. Mtg., Soc. Expl. Geophys., Expanded Abstracts, 293-296.

Narville, C., 1986, Detection of anisotropy using shear-wave splitting in VSP surveys: requirements and applications: 56th Annual SEG meeting, Expanded Abstracts, 391-394.

Peron, J. 1990, Estimation of fracture directions from zero-offset VSP by two- and four-component rotation: 60th Annual SEG Meeting, Expanded Abstracts, 1443-1446.

Rathore, J.S., Fjaer, E., Holt, M. and Renlie, L., 1991, Experimental versus theoretical acoustic anisotropy in controlled cracked synthetics: 61th Internat. Mtg., Soc. Expl. Geophys., Expanded Abstracts, 687-690.

Rümpker, G., Brown, R.J. and Thomson, C.J., 1996, Shear wave propagation in orthorhombic phenolic: a comparison of numerical and physical modeling: J. Geophy. Research, 101, 12, 27,765-27,777.

Schulte, L., and Edelmann, H.A.K., 1988, Azimuthal anisotropy proven to be a useful approach for multicomponent shear-wave data processing: 58th Internat. Mtg., Soc. Expl. Geophys., Expanded Abstracts, 1156-1158.

Stewart, R.R., 1994, Proposal for continuation (1995) of the CREWES Project: CREWES Project, The University of Calgary.

Thomsen, L., 1986, Weak elastic anisotropy: Geophysics, 51, 1954-1966.

Thomsen, L., 1988, Reflection seismology in azimuthally anisotropic media: Geophysics, 53, 304-313.

Winterstein, D.F., 1989, Comparison of three methods for finding polarization direction of fast shear-wave: SEG research workshop, Snowbied, Utah, Technical Abstracts, 118-119.

Winterstein, D.F., 1990, Velocity anisotropy terminology for geophysicists: Geophysics, 55, 1070-1088.

Winterstein, D.F., and Meadows, M.A., 1991, Changes in shear-wave polarization azimuth with depth in Cymric and Railroad oil fields: Geophysics, 56, 1349-1364.

Yang, G.Y.C., 1996, 9C-2D seismic data analysis: Olds, Alberta: CREWES Report 1996, CREWES Project, The University of Calgary, Alberta.

Zhang, Y., 1995, Short window minimax norm optimization for multisource multicomponent S-wave data in the presence of azimuthal anisotropy: 65th Internat. Mtg., Soc. Expl. Geophys., Expanded Abstracts, 360-363.